1991

Experimental and analytical investigations of a folded plate model bridge

Taher Merchant
Iowa State University

Experimental and analytical investigations of a folded plate model bridge

by

Taher Merchant

A Thesis Submitted to the
Graduate Faculty in Partial Fulfillment of the
Requirements for the Degree of
MASTER OF SCIENCE

Department: Civil and Construction Engineering
Major: Civil Engineering (Structural Engineering)

Iowa State University
Ames, Iowa
1991

TABLE OF CONTENTS

1. INTRODUCTION

Bridge closed! An irritating sign for any traveller, is threatening to become a very common sign. Due to lack of maintenance, increases in the design load specifications set forth by the American Association of State Highway and Transportation Officials (AASHTO) [1], and increased traffic volumes, thousands of deficient bridges need to be replaced, strengthened or repaired. Closing a large number of bridges or posting them for reduced loads can disrupt any country's surface transportation system. Out of approximately 578,000 highway bridges in the United States 39.9% have been rated deficient or functionally obsolete [2]. The closing of a bridge for maintenance or emergency repairs always causes costly delays and inconvenience to the travelling public. The problems are more severe when the bridge is serving a high volume of traffic or is isolated from other bridges. Maintaining traffic and eliminating detours is a difficult problem faced by various bridge departments all over the country. Needed today is an alternative bridge system which is capable of supporting current traffic volumes and is economical and fast to construct.

Prefabricated elements and systems offer a popular and convenient solution for replacing damaged and deficient bridges fast and at a relatively low cost. Many such elements and systems are presently available. Precast, prestressed concrete units such as prestressed beams and slabs have been used for short span bridges, i.e., those that require no intermediate support. In situations where longer spans are needed, these units require one or more intermediate supports; however the construction of intermediate supports is

costly and cannot be accomplished in a short period of time. The main obstacle in the use of precast prestressed elements for longer spans without intermediate supports is the difficulty in handling, transporting and placing the heavy, long concrete elements. This difficulty of dealing with large size precast elements was overcome when the technology for segmental construction of precast concrete box girder bridges was introduced by Freyssinet Organization in the 1960's in France [3]. In this method smaller precast elements are assembled together and post-tensioned on site to bridge longer spans.

Arches are an ancient and economical method of bridging long spans. An arch was a very common structural system used to transfer loads to supports primarily by axial compressive forces. As concrete has excellent compressive strength, it is an ideal material for arches. Arches need strong abutments as springers and thus are not suitable for all locations. With speed of construction, economy of cost and ability to cover long spans as the objective a new idea for an alternate bridge system has been developed and investigated at Iowa State University.

An integrated deck and shell structure which combines the advantages of prefabricated element systems and segmental construction, has high torsional rigidity like a box girder bridge, and arch action in the transverse direction was investigated for use as a bridge. Preliminary investigations were completed by Andrey [3]. In this study, fifteen different cross sections were analyzed. From these, four different configurations of an integrated deck and circular shell structure along with curbs and shell edge beams were studied in detail using the finite element technique. The effect of the width of

the shell-deck connection was also studied. Cross-sections with both narrow and wide shell-deck connections were analyzed; it was determined that a wide shell-deck connection reduced the transverse stresses in the deck but increased the self weight of the structure. Andrey [3] also investigated an integrated deck and folded plate structure and compared it with the integrated deck and circular shell structure. The folded plate-deck structure showed an overall improvement over the circular shell-deck structure except in the transverse direction because no arch action exists in the folded plate deck structure which results in higher transverse stresses. Another advantage with folded plate structures is that the formwork needed to build them is easier to construct than that necessary for a circular shell structures. To calibrate the analytical work done by Andrey [3] and to further investigate the structural behavior of integrated shell-deck and folded plate-deck bridges two scaled models were constructed and tested. The first model was a 1:3 scale 6 segment prestressed concrete model of an integrated deck and circular shell structure, the study of which is presented by Wassef [4]. The other was a 1:24 scale Plexiglass model of an integrated deck and folded plate bridge, the study of which is presented herein.

Even though using folded plate structures for bridges is a new concept, folded plate roof structures have been used extensively where longer span lengths are required. To cover very long spans even prestressed folded plate structures have been constructed. Several authors have presented approximate analyses techniques for prestressed folded plates, and even some model studies of prestressed folded plates have been conducted. Some work

done in this field has been presented in papers by Klaiber, Gutzwiller and Lee [5], Brough and Stephens [6], Glanville [7] and Goble [8].

The objective of the work presented herein is to experimentally and analytically investigate the response of an integrated deck and folded plate structure. Listed below are the various tasks completed to achieve this objective:

1. Design and construct a scaled model of an integrated deck and folded plate structure using Plexiglass as the main model material.
2. Investigate the physical properties of Plexiglass such as the modulus of elasticity and Poisson's ratio by performing tests on samples of Plexiglass used in the model.
3. Determine the approximate post-tensioning force required using simple beam theory and allowing no longitudinal tensile stresses in the model.
4. Select appropriate strain gages and install them on the Plexiglass bridge model and the post-tensioning tendons.
5. Calibrate the post-tensioning tendons.
6. Test the bridge model using a single concentrated load for two configurations-with and without 6 diagonal truss members connecting the curb and the beam.
7. Apply the predetermined post-tensioning force and repeat the above tests.
8. Perform sensitivity analysis for determining the most economical size of the three dimensional finite element isoparametric solid element and develop a finite element model of the structure for each

of the following configurations; with no diagonals, 6 diagonals and 12 diagonals connecting the beams and the curbs.

9. Analyze the structure using the finite element model for a single concentrated load and AASHTO [1] loading placed at predetermined locations.
10. Compare the experimental and analytical results and verify the finite element modelling of the structure.

2. MODELLING AND MODEL CONSTRUCTION

Advances made in the computer technology has made it possible for considerable research work to be done with theoretical or mathematical models; despite this the researcher in the field of engineering cannot relieve himself totally from experimentation. Scaled models are useful in supplementing and calibrating mathematical models.

This experimental model study was conducted to investigate the elastic response of the integrated deck and folded plate structure to static loads as well as to provide data for calibrating the finite element model which assumes a homogeneous, isotropic and linear elastic material.

2.1. Model materials

Plastics and metals are the most commonly used materials for the fabrication of elastic models [9]. Both these materials have their characteristic advantages and disadvantages. Even though metals have stable elastic properties and are relatively insensitive to thermal effects, plastics are more popular for modeling. Plastics are easier to fabricate into complex structures and configurations; also, because of their higher elastic modulus metals require relatively larger loads to produce measurable strains.

The commonly used plastics are thermoplastics and thermosetting plastics. Thermoplastics can be formed after being heated to a softening temperature (200^{0}F-300^{0}F); thermosetting plastics however cannot be softened by heating once the material is formed [9].

The material used to construct the model for this study is Plexiglass. Chemically known as Polymethyl methacrylate, Plexiglass is a thermoplastic [10]. The physical properties of Plexiglass vary; the modulus of elasticity being between 400,000 and 500,000 psi. Poisson's ratio is approximately 0.35 and the coefficient of thermal expansion is between $4x10^{-5}$ to $5x10^{-5}$ per^{0}F. The material is a very poor electrical and thermal conductor. Plexiglass was selected for use in this investigation to take advantage of the above listed properties of plastics in the manufacturing the model. Along with the above advantages, Plexiglass also has the following disadvantages.

- A modulus of elasticity of about 500,000 psi is in the right range for convenient use in models, but Plexiglass exhibits high creep and the modulus of elasticity is time dependent. According to Hood [11] the modulus of elasticity is also very sensitive to temperature changes.
- A high Poisson's ratio, 0.35, does not compare very well with the 0.15-0.2 of concrete. Care must be taken in the interpretation of model test results where Poisson's ratio may affect the behavior.
- Low thermal conductivity limits the number of available strain gages, and also causes gage heating at high operating voltages thus affecting the accuracy of strain measurements.

As physical properties of Plexiglass are found to vary from sample to sample, it has been suggested that these material properties be evaluated before each investigation by conducting tests on samples of Plexiglass used in the model [9].

To determine the modulus of elasticity and Poisson's ratio of the Plexiglass used in the construction of the model, a beam test was set up as

shown in Figure 2.1. Two strain gages, perpendicular to each other, were installed on each of the top and bottom faces of the beam. One measured the longitudinal and the other the transverse strain in the beam. The gages were read using a data acquisition system programmed to pause for 10 seconds after each recording. An additional 4 seconds were utilized in printing the measured strains, thus the strain gages were read and recorded every 14 seconds. The load, W, along with the loading apparatus was varied from 3.23 lb to 7.23 lb. Thus varying the stress in the top and bottom fiber of the beam from 213 psi to 477 psi.

Figure 2.2 shows the variation of strain with respect to time at a constant stress of 213 psi. As can be noticed, the rate of creep reduces after the first minute, however Preece and Davies [9] concluded that for the creep rate to become negligible it takes approximately six hours. Fortunately, it was observed that the rate of creep is independent of stress at stress levels normally encountered in models. A curve similar to that shown in Figure 2.2 was obtained when change in strain with respect to time was plotted for a constant stress of 477 psi.

As can be observed from the variation in strain at constant stress, the strain in the Plexiglass beam increases with time elapsed after loading. The ratio of stress to measured strain i.e., the modulus of elasticity of Plexiglass, calculated instantly after loading, one and two minutes from loading was 443,800 psi, 414,900 psi and 409,700 psi, respectively. The value of modulus of elasticity used for this study was 443,800 psi; for all testing the strains were read instantly after loading as soon as possible. The time interval between two consecutive load tests was at least 10 minutes to allow for creep recovery.

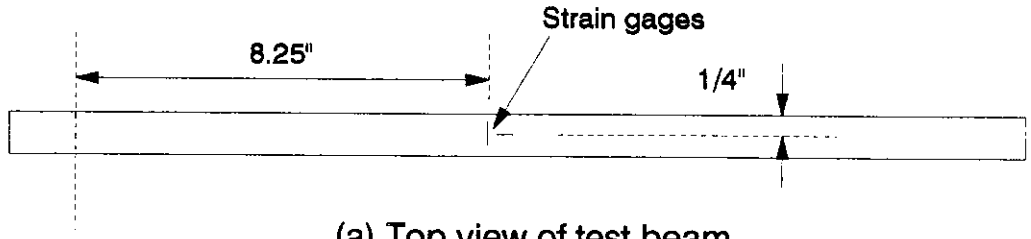

(a) Top view of test beam

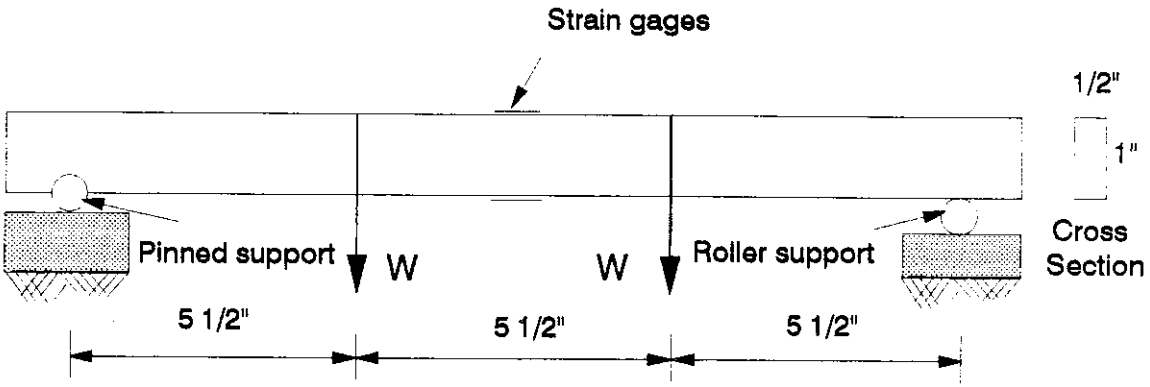

(b) Side view of test beam

Figure 2.1. Beam test arrangement for determining Young's modulus and Poisson's ratio for Plexiglass

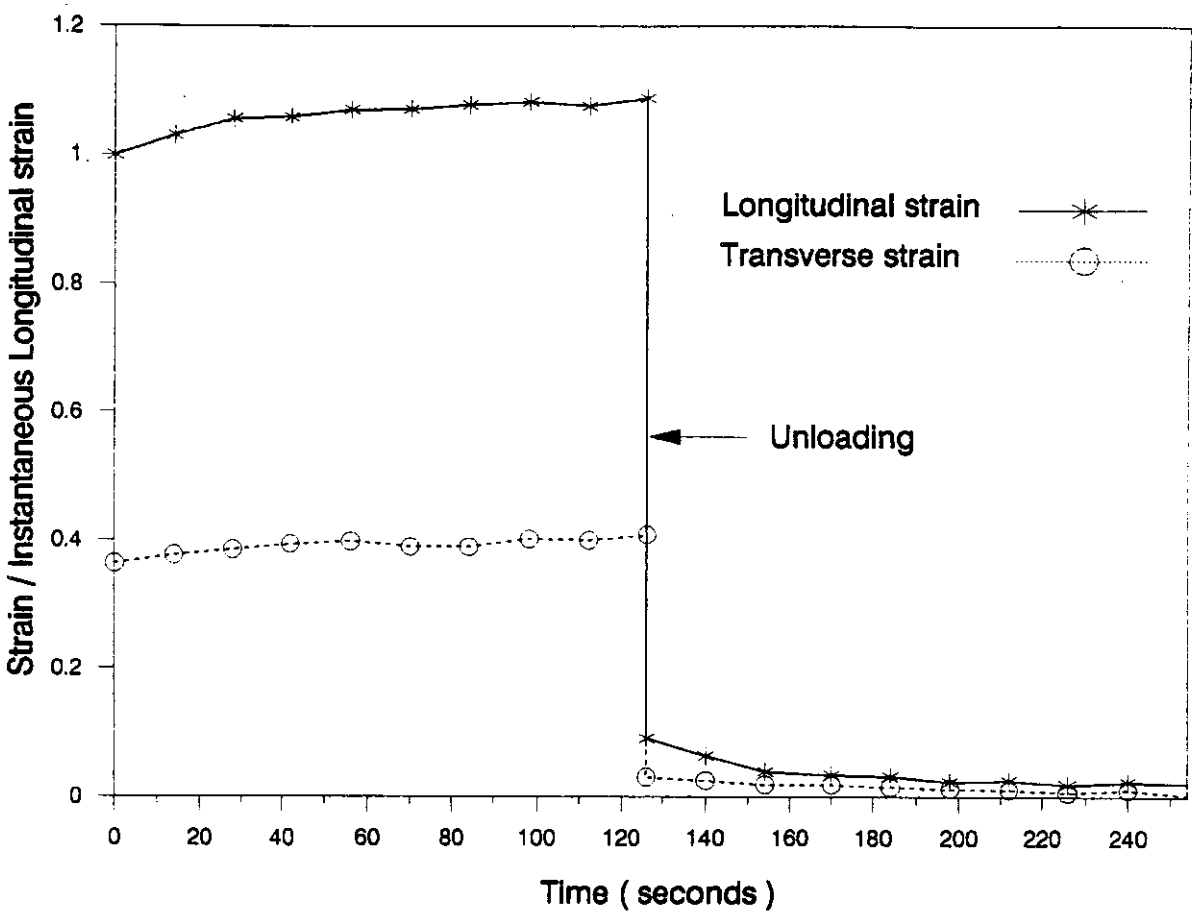

Figure 2.2. Time dependent strains in prismatic beam under a constant stress of 213 psi

From the stress and instantaneous strain relationship shown in Figure 2.3, one can conclude that the material is linearly elastic up to a stress of at least 477 psi. The stresses in the Plexiglass model were neither anticipated nor measured to be higher than this value, thus Plexiglass is suitable for elastic modeling. The value of Poisson's ratio as determined from the beam test was 0.36.

2.2. Similitude of modeling

The purpose of models is to reduce the time and cost of exploring new ideas, solving technical problems and improving designs. To fulfill this purpose one should be able to extrapolate the test results from the model to the prototype. Extrapolation of results from model to prototype can be done only if there exists a definite relationship between the geometry of the model and the prototype and the loads applied on the model and those that would be experienced by the prototype.

2.2.1. Scaling of a model

The basic idea in similitude is to have similarity between the prototype and the model. This is achieved by applying the Buckingham Pi Theorem [12] that relates all quantities like the dimensions, material properties and loads of the model with those of the prototype. The theorem states that the number of dimensionless and independent quantities called Pi (π) terms, needed to express a relationship between model and prototype is equal to the number of quantities involved minus the number of basic dimensions in which the quantities may be measured. This is expressed as:

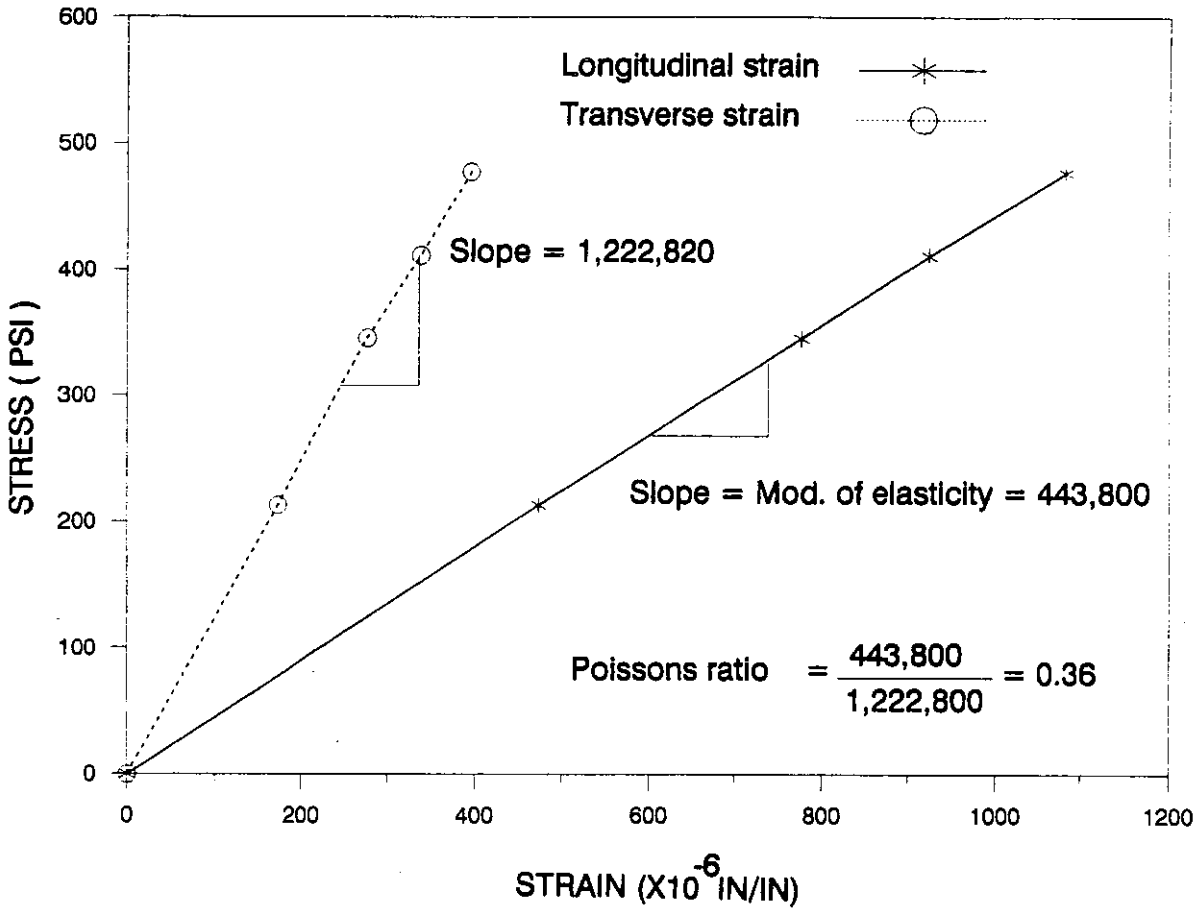

Figure 2.3. Variation of stress versus instantaneous strains

$$s = n - b \qquad (1)$$

where s = number of Pi (π) terms

n = total number of quantities involved

b = number of basic dimensions involved.

Equating the Pi terms for the model and the prototype, one gets :

$$X_m = \frac{l_m}{l_p} X_p \qquad (2)$$

where X_m and X_p are corresponding dimensions of the model and the prototype, respectively. The variables l_m and l_p are the length of the model and prototype respectively. The factor l_p/l_m is known as the length scaling factor S, and any dimension of the model can be obtained by utilizing this factor.

2.2.2. Scaling of loads

The scaling of loads to be applied on the model is done similar to the scaling of model dimensions, by applying the Buckingham Pi Theorem. The various quantities involved here are:

l_m and l_p = length of the model and prototype, respectively.

E_m and E_p = Modulus of elasticity of model and prototype, respectively.

ε_m and ε_p = strains in the model and prototype, respectively.

σ_m and σ_p = stresses in the model and prototype, respectively.

w_m and w_p = Distributed loads on model and prototype, respectively.

P_m and P_p = Concentrated loads on model and prototype, respectively.

ρ_m and ρ_p = Weight density of model and prototype, respectively.

ν_m and ν_p = Poisson's ratio of model and prototype, respectively.

The various Pi terms, dimensionless and independent quantities are:

$$\varepsilon, \quad \nu, \quad \frac{El}{w}, \quad \frac{El^2}{P}, \quad \frac{E}{\rho l}, \quad \frac{E}{\sigma}$$

Equating the Pi terms for the model and the prototype, one gets:

$$\varepsilon_m = \varepsilon_p \tag{3}$$

$$\sigma_m = \frac{E_m}{E_p}\sigma_p \tag{4}$$

$$w_m = \frac{E_m}{E_p}\frac{w_p}{S} \tag{5}$$

$$P_m = \frac{E_m}{E_p}\frac{P_p}{S^2} \tag{6}$$

$$\rho_m = \frac{E_m}{E_p}\frac{\rho_p}{S} \tag{7}$$

$$\nu_m = \nu_p \tag{8}$$

where, S is the length scaling factor.

Using equations (5) and (6), the loads to be applied on the model were calculated. Equations (3) and (4) express the relationship between the stresses and strains in the model and prototype. The weight density of the model material, in this case Plexiglass, is less than the value obtained from equation (7). Hence, to compensate for the lesser self weight of the model, additional distributed load could be used. The inequality in the Poisson's ratio of Plexiglass and concrete, the model and prototype materials, has been discussed in section 2.1 and its effect is explained in section 5.2.1.

2.3. Model geometry and construction

For this study a 1:24 scale model of a two lane, single span, simply supported, integrated deck and folded plate bridge was constructed and tested. This scale factor was selected so that a deck thickness of 6 in. can be conveniently modeled with a single sheet of Plexiglass 0.25 in. thick. Several types of sections were theoretically analyzed and compared by Andrey [3]. Figure 2.4 illustrates several views and the arrangement of the post-tensioning tendons on the bridge model tested. The dimensions of the prototype and the scaled model are tabulated in Table 1.

The model was fabricated in the Engineering Research Institute machine shop at Iowa State University. The edge beams at the bottom were cemented to the inclined web plates and the web plates in turn were cemented

Table 1. Dimensions of model and prototype

Dimension	Prototype	Plexiglass Model (1:24)
1) Span length	100'	50"
2) Width of bridge (2 lane)	30'	15"
3) Thickness of bridge deck	6"	1/4"
4)Thickness of folded plates	4-1/2"	3/16"
5)Curb size	15" x 21"	5/8" x 7/8"
6) Bottom beam size	18" x 24"	3/4" x 1"
7) Thickness of diaphragm	12"	1/2"

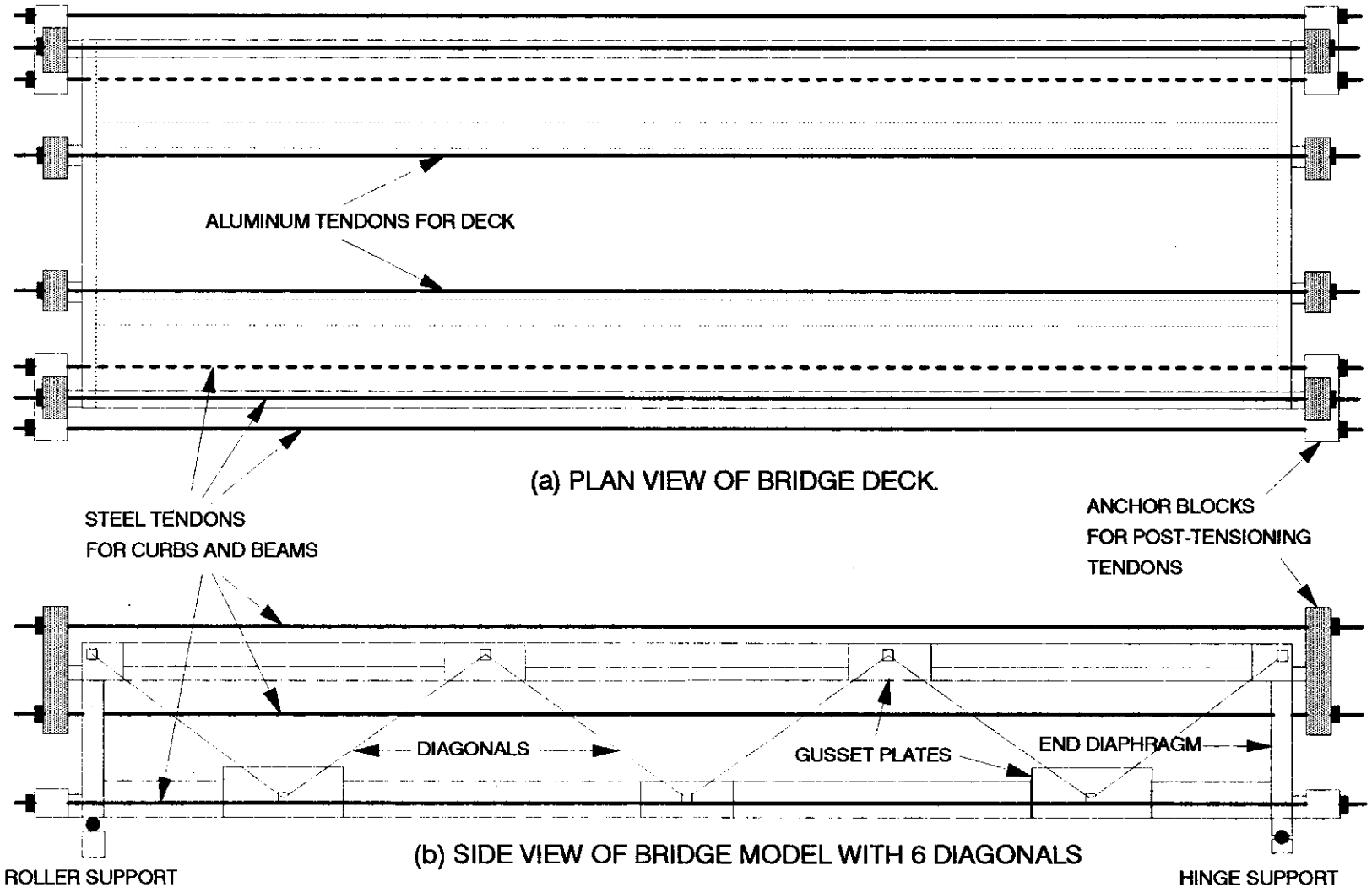

Figure 2.4. Illustration of the Plexiglass bridge model

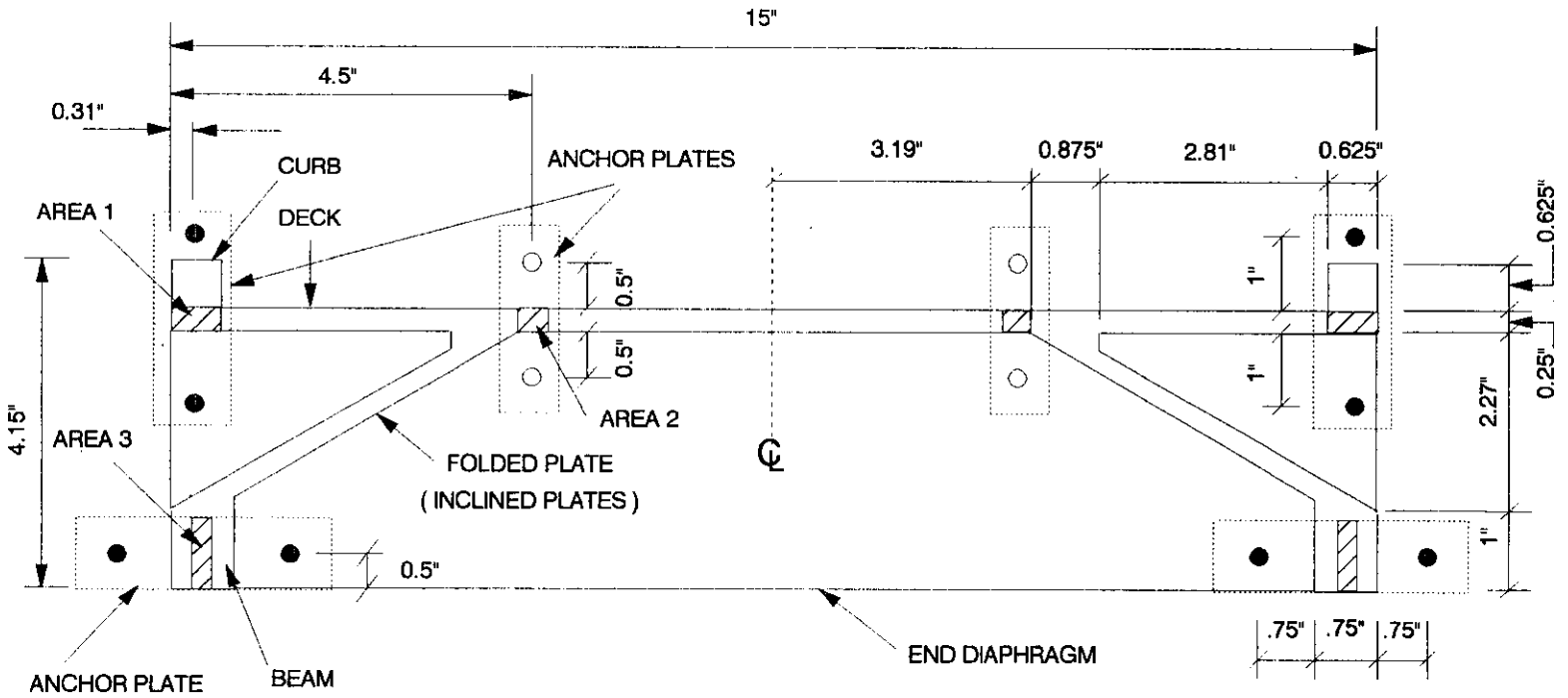

(c) CROSS SECTION OF BRIDGE MODEL

Figure 2.4. (continued)

to the deck forming a folded plate deck cross section (see Figure 2.4). The cement used was WELD ON #3 (fast cure, Acrylic glue) and the cementing procedure cemented the different parts so that they acted monolithically (i.e. like a folded plate with stiffened edges). The curbs were mechanically attached with bolts to the deck so that the model could be tested with and without the curbs. Curbs and the beams were connected by diagonal members to obtain an integrated truss action. Aluminum gusset plates were initially used to connect the diagonals to the beams and the curbs. However it was impossible to exactly scale down the thickness of the gusset plate from the prototype to the model. The 0.125 in. thick aluminum gusset plates stiffened the model to such an extent that it lost its geometric similarity with the prototype. Since it was not practical to further reduce the thickness of the gusset plates, it was decided to replace the aluminum gusset plates with Plexiglass gusset plates. This helped in reducing the stiffness of the gussets by a factor of 22.5, which is the ratio of the elastic modulus of aluminum and Plexiglass.

The prestressing force was applied by tensioning the twelve symmetrically placed tendons shown in Figure 2.4. Four of these post tensioning tendons were of aluminum and the rest were steel. Their inherent advantages and disadvantages are discussed in the next section.

The size of the model made it easy to test the behavior of the model with and without the diagonals. At the same time the small size of the model prevented the use of additional diagonals to obtain better truss action between the curbs and the beams.

2.4. Post-tensioning tendons

Initially all the post-tensioning tendons were 3/8" diameter plain aluminum tendons with a fine threading of 32 threads per inch at both ends. The tension in the tendons applied the prestressing force to the model. The tension in the tendons was measured by monitoring the strains in the tendons. Two strain gages were fixed longitudinally and diametrically opposite on each of the post-tensioning tendons. The small size of the gages made it difficult to align the axis of the gage exactly parallel to the axis of the tendon. This imperfection in installation of the gages causes strain readings to differ in bars carrying the same force. Hence it was necessary to calibrate each tendon using the simple tension test shown in Figure 2.5. Though initially it seemed necessary to calibrate the tendons, it was observed that the difference in the measured strains due to misalignment of the strain gages on the tendons when subjected to the same load was negligible. Therefore, for the new set of tendons calibration was not required.

The testing of the model required that the tendons be tensioned and released several times, and even though the tendons were annealed for surface hardening, the threads would wear out and render the tendon useless. Using stronger threads with a pitch of 24 threads per inch instead of 32 threads per inch did not improve the resistance to wear. However the use of coarser threads reduced sensitivity while tensioning i.e., for each revolution the nut travelled a larger distance and induced a larger force in the tendon.

Finally changing from aluminum to steel tendons not only increased the strength of the threads and their resistance to wear, but reduced relaxation

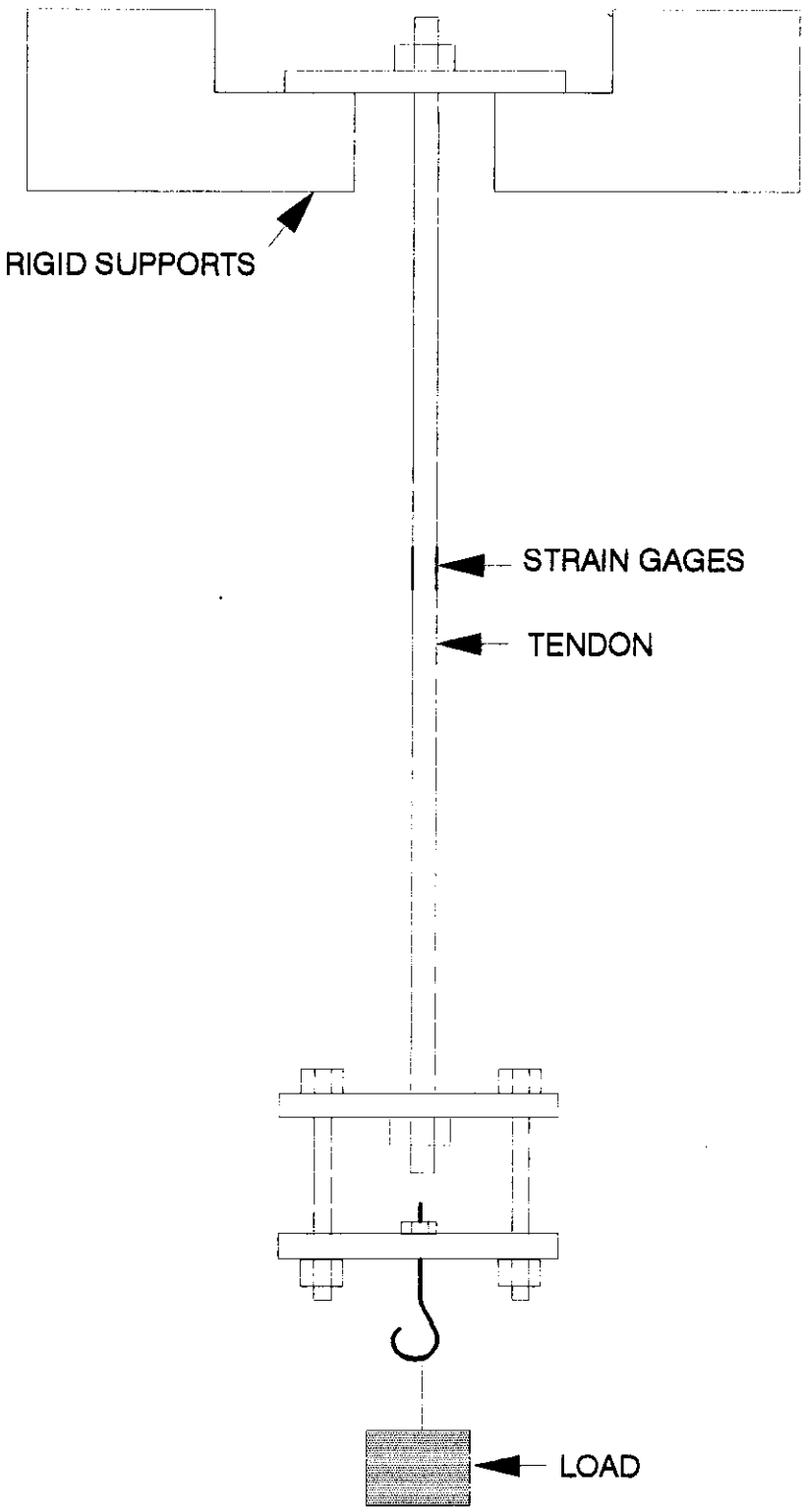

Figure 2.5. Arrangement for callibrating post-tensioning tendons

losses. It was determined that relaxation in steel tendons was much less than in aluminum tendons, thus steel tendons could sustain the prestressing force for a longer period of time. The disadvantage with using steel tendons is that they have a higher modulus of elasticity and hence require smaller strains to apply the same force, and the percentage error in the measurement of small strain could be greater.

2.5. Determination of post-tensioning forces

Even though the Plexiglass model was a complete single span unit by itself, the prototype would have to be constructed in smaller segments which would then be joined together by applying post-tensioning force. Segmental construction would then require that no longitudinal tensile stress be allowed at any service load.

For the purpose of determining the required post-tensioning force, the bridge structure was treated as a simple beam, having sectional properties similar to the following sectional properties of the bridge :

- Cross sectional area of the section = 8.1 in^2
- Moment of inertia of section = 11.8 in^4
- Total depth of section = 4.15 in
- Distance of centroid of section from top fiber = 1.56 in

From load simulation discussed in Section 2.2.2, it was determined that the scaled dead load of the model should be 2.0 lb/in. This would give a maximum moment of 648 in-lb at midspan due to dead load alone. The maximum moment due to live load was calculated using the HS20-44 lane loading [1]. An

impact factor of 1.22 determined from AASHTO [1] was applied to the live load. The total maximum moment due to the scaled service live and dead loads on the model was calculated to be 974.4 in-lb.

The prestressing force on the model is applied in two regions, at the top, in the deck and the curb, and at the bottom, in the beams (see Figure 2.4). Using beam theory and assuming that no longitudinal tensile stresses are allowed in the model under dead and live loads, the following post-tensioning forces were determined:

245 lb. shared equally by 8 tendons in the deck and the curbs; i.e. 30.6 lb. per tendon.

372 lb. shared equally by 4 tendons in the beams; i.e. 93 lb. per tendon.

3. MODEL INSTRUMENTATION

Basic instrumentation on the model consisted of electric resistance strain gages (henceforth referred to as gages) for measurement of strains and mechanical dial gages for measuring deflections. As with the test beam (see section 2.1) strain gages were read using a Hewlett Packard data acquisition system (DAS).

3.1. Selection of strain gages

The initial step in preparing for any strain gage installation is the selection of an appropriate gage for the task. Selection of the proper gage is important in optimizing the gage performance and can be accomplished by considering the following gage parameters:

i) Strain sensing alloy for the gage element.

ii) Backing (carrier) material for the gage.

iii) Gage length.

iv) Gage pattern.

v) Self temperature compensation characteristic.

vi) Grid resistance.

vii) Gage connection options.

Micro Measurements, a leading manufacturer of strain gages has suggested that for a general purpose static stress analysis test where the strains are not very large (no post yield testing) and fatigue life is not an important criterion, a Constantan foil gage with a polymide backing may be

used [13]. As the model testing was conducted under constant temperature conditions, the temperature compensation characteristics of the gages were not critical. However, for materials with specific thermal expansion coefficients like the aluminum and steel tendons, self temperature compensated gages are available with STC numbers 13 and 06 respectively [13].

Strain gages are commonly available in two different resistances, 120 ohms and 350 ohms. The data acquisition system which was used to monitor the gages could only read gages with 120 ohm resistance, hence 350 ohm gages could not be used.

The gage length and the gage pattern should be selected on the basis of the anticipated strain gradient and the nature of the strains. However, when Plexiglass is the model material, the size of the gage is also controlled by the need to avoid gage heating. To avoid gage heating, the heat generated within a strain gage must be transferred by conduction to the mounting surface and dissipated to the atmosphere. The heat generated in a gage is directly proportional to the power consumed in the gage. For any given gage resistance, the heat generated is higher for higher excitation voltages. Since plastics act as thermal insulators, a high excitation voltage will result in excessive self heating of the gage and in the degradation of the gage's performance. At the same time, low excitation voltages will result in loss of accuracy in strain measurement. Hence, an optimum excitation voltage has to be selected depending on the following three factors:

- Gage resistance
- Thermal conductivity of substrata
- Strain gage grid area.

The procedure outlined in Reference [14] was used to assist in the selection of strain gages to minimize gage heating.

3.2. Types of gages

The gages selected for recording strains in the bridge model were

- EA-13-125BT-120.....for use on the aluminum post-tensioning tendons.
- EA-06-125BT-120.....for use on the steel post tensioning tendons.
- EA-06-250BG-120.....for use on the Plexiglass model.

EA-13/06-125BT-120: These are general purpose gages with narrow grid and compact geometry suitable for installation on 3/16 in. diameter post-tensioning tendons. The gages are 0.125 in. long and 0.062 in. wide. These are Constantan foil gages mounted on a tough, flexible cast polymide backing film.

EA-06-250BG-120: This is also a general purpose Constantan foil gage on a polymide backing with a compact geometry. It has a gage length of 0.25 in. and a grid width of 0.125 in. giving a grid area of 0.03125 in^2. When this gage is mounted on a poor heat conductor like Plexiglass and moderate accuracy is desired, the excitation voltage should not be greater than 0.85 volts [14] to avoid excessive gage heating.

A simple drift test was performed to determine the maximum allowable excitation voltage which would not result in gage heating and excessive drift. After installation of all the strain gages on the model, power was supplied to the gages and the strains were read at intervals of 10 minutes for zero load on the model. Figure 3.1 illustrates the average drift from the zero value in all the gages with respect to time for two different operating voltages. The average drift was obtained by monitoring the drift in 15 gages selected at random from

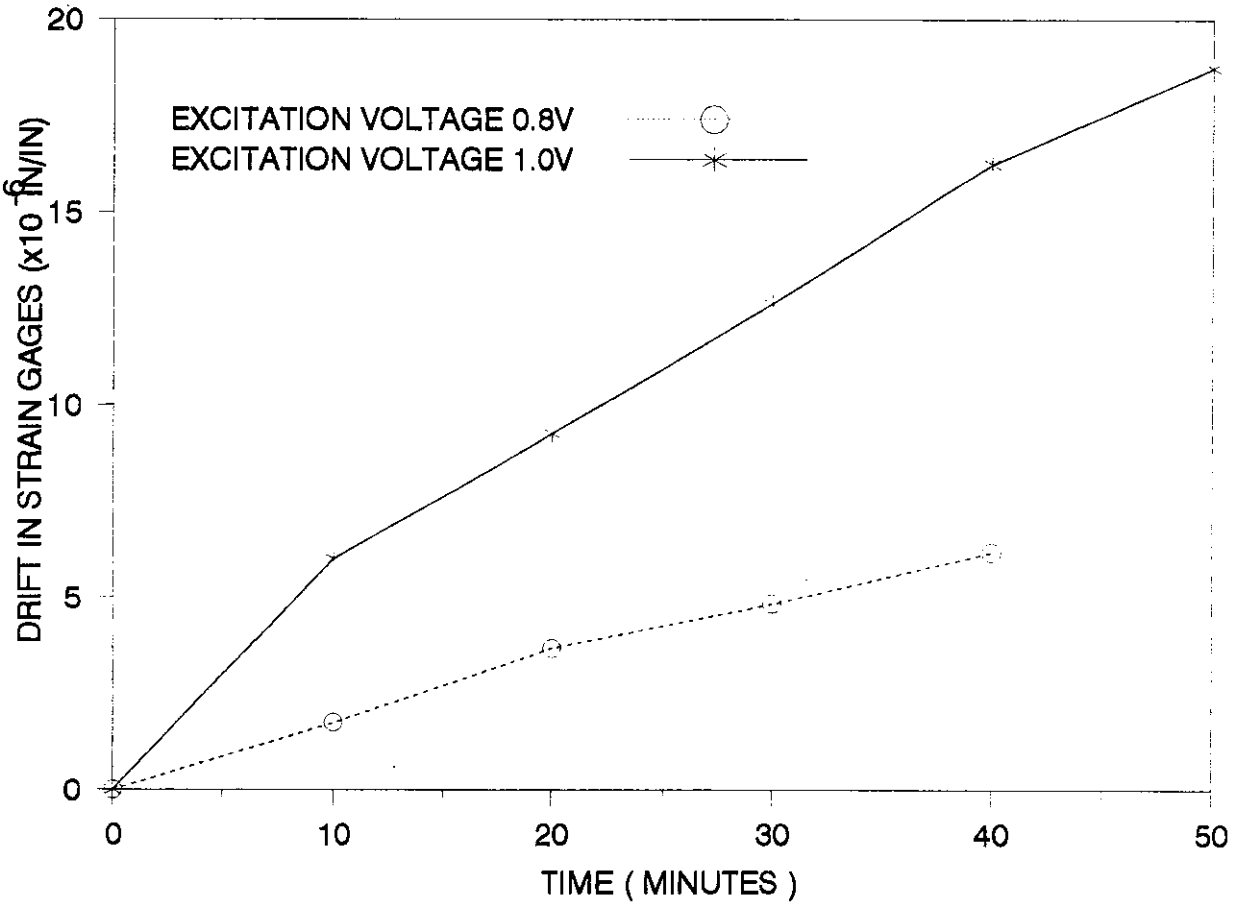

Figure 3.1. Average drift in strain gages with time

the 70 gages installed on the bridge. As can be observed from Figure 3.1, for an increase of 0.2 volts in the excitation voltage, the average drift in the gages increased three fold. At an excitation voltage of 0.8 volts, the average drift in the gages was observed to be 6×10^{-6} in/in after 40 minutes. Sufficiently accurate strain measurements can be obtained when the strains being measured are large, however the reliability and accuracy of strain measurements is reduced in regions of low strains where the measured strain is comparable to the drift in the strain gages.

3.3. Distribution and installation of gages

The model is geometrically symmetric about the longitudinal and transverse axes, and hence one can assume that its response under symmetrical loads would be symmetric. Taking advantage of the symmetry, strain gages were installed on only one quarter of the bridge. To check the symmetrical behavior of the bridge, 10 gages were installed in the remaining three quarters of the bridge. Gages were positioned so that the strains could be monitored along the top and bottom of the curb and the beam, the longitudinal and transverse center lines of the deck, and near the deck and the web connection. The location of the gages on the different parts of the bridge model is shown in Figures 3.2a-3.2d.

As will be shown, only longitudinal strains in the curbs and the beams are prominent and the transverse strain is negligible. Hence, strain gages were installed only in the longitudinal direction for the curbs and the bottom beams. However, in the deck, two separate gages perpendicular to each other were installed at each point of interest to measure the longitudinal and the

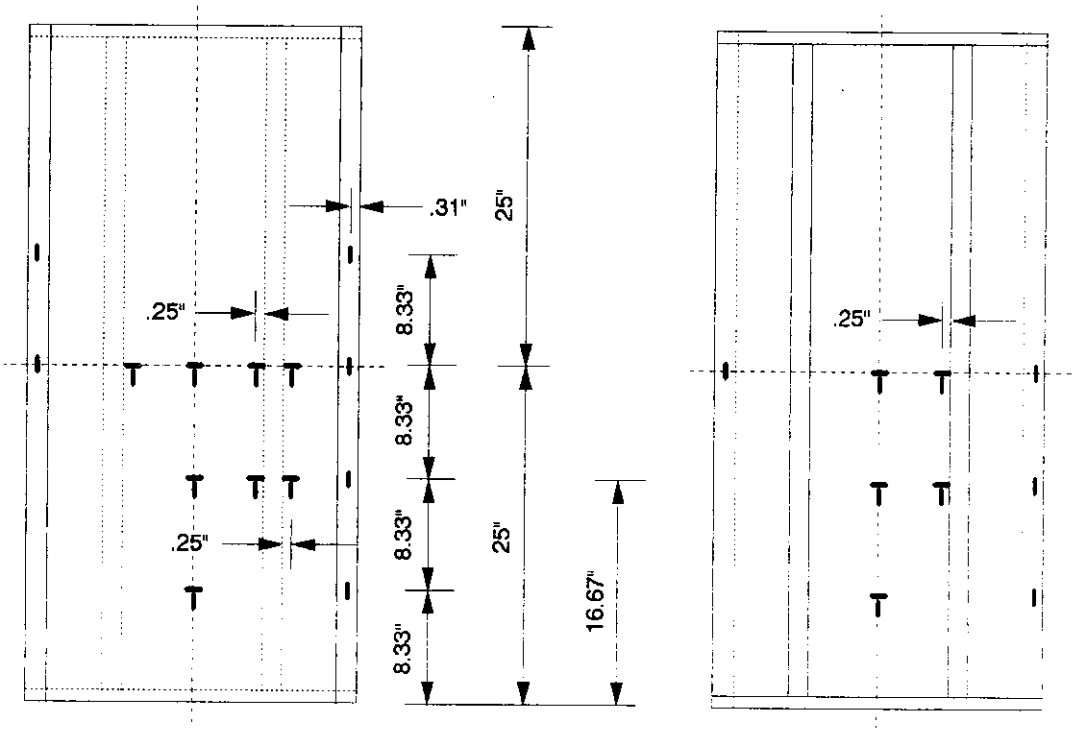

(a) TOP OF DECK AND CURBS

(b) BOTTOM OF DECK AND CURBS

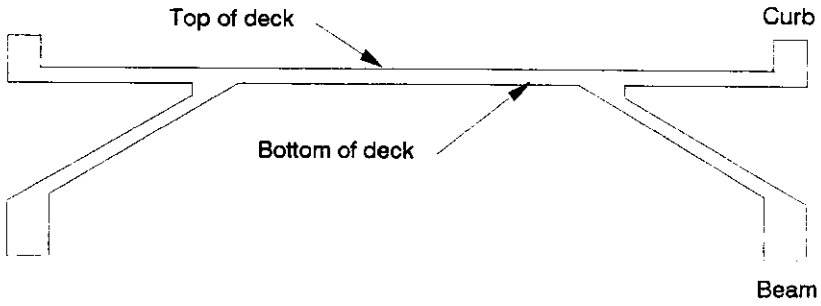

CROSS SECTION VIEW

Figure 3.2. Location of strain gages in different parts of the bridge model

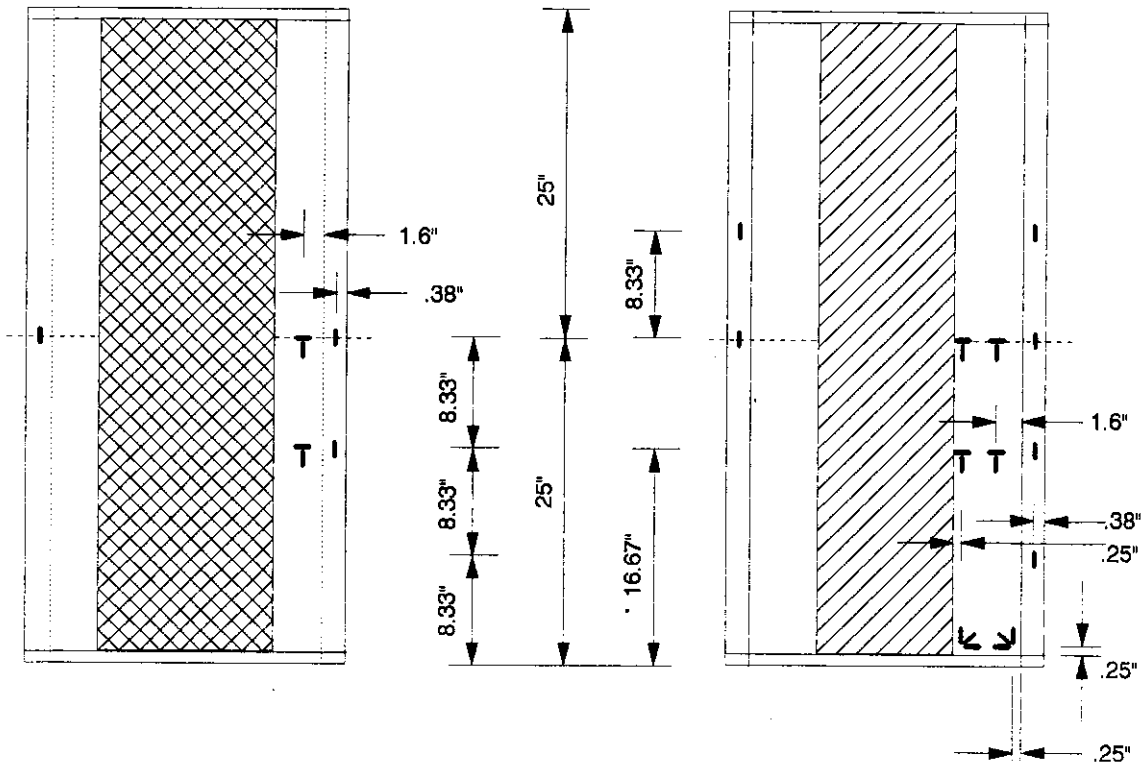

(c) TOP OF FOLDED PLATE AND EDGE BEAMS

(d) BOTTOM OF FOLDED PLATE AND EDGE BEAMS

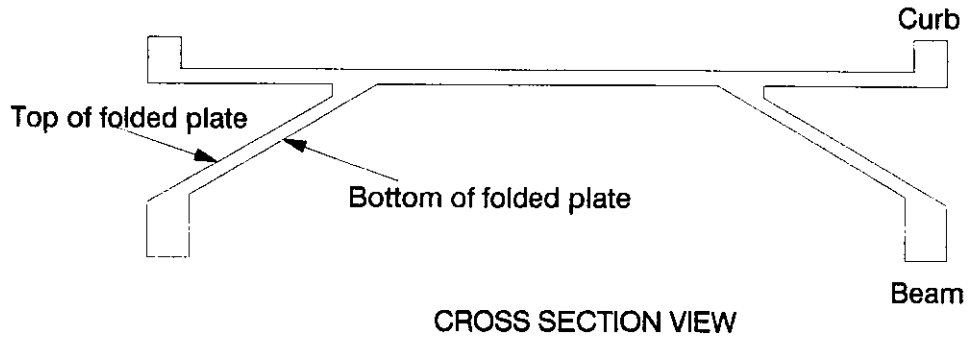

CROSS SECTION VIEW

Figure 3.2. (continued)

transverse strains. This combination was used instead of using a two arm Tee rosette to avoid gage heating problems.

Installation of gages was carried out strictly according to the manufacturers (Micro Measurements) guidelines. The adhesive used to install the gages was M-Bond 200, a special grade of methyl-2- cyanoacrylate. It is a general purpose adhesive, cures almost instantly and produces an essentially creep free, fatigue resistant bond between the gage and the mounting surface. Each gage was labelled in a predetermined sequence and tested. Once the connections were checked, each gage was coated with a thin layer of protective coating to protect the gage from damp or wet conditions. The protective coating used was 3140 RTV, whose main constituent is silicone rubber. It forms a translucent, non-corrosive tough rubber like coating which cures at room temperature in about 24 hours.

Mechanical dial gages were used to measure the deflections of the beams and the curbs at midspan. Due to space limitations, more dial gages could not be placed, hence the measured strains have been prominently used for analyzing the behavior of the bridge structure.

4. FINITE ELEMENT ANALYSIS

4.1. Finite element software

The integrated deck and folded plate structure was analyzed using the ANSYS [15] general purpose finite element program. ANSYS has been previously used and verified in similar kinds of studies Andrey [3] and Wassef [4]. This resulted in saving time in software validation and appropriate element type selection.

The quadrilateral shell element and the three dimensional isoparametric solid element (STIFF 63 and 45 in the ANSYS element library) were investigated by Andrey [3] for use in the modelling of integrated deck and shell structures. Andrey concluded that solid elements with a fine mesh in the transverse direction was adequate to ensure a sufficient representation of the actual structural behavior. Even though solid elements required a finer mesh and more computation time, their use resulted in a realistic modelling of the integrated deck and folded plate structure.

The three dimensional isoparametric solid is an eight node element with three degrees of freedom at each node, translations in the nodal x, y and z directions. The co-ordinate system of the element is set parallel to the global co-ordinate system to facilitate retrieving the data in the post-processing phase. Loads can be applied as nodal forces or pressures on element faces. The element theory is based upon a formulation which includes modified extra displacement shapes, the advantage of which is explained in the following section. ANSYS uses a 2x2x2 lattice of integration points with the Guassian

numerical integration procedure employed in calculating the element stiffness matrix [15].

4.2. Finite element model

Figure 4.1 illustrates the finite element mesh of the deck-folded plate bridge structure (1/4 of model illustrated). Again taking advantage of the geometric symmetry of the model about both the longitudinal and transverse axes, a considerable amount of computation time was saved by modelling only one quarter of the bridge. Both symmetric and unsymmetric loading cases can be analyzed by specifying symmetric or asymmetric boundary conditions along the cut edges and adding results from different loading cases. The Global X, Y and Z co-ordinate axes are as shown in Figure 4.1.

Three dimensional isoparametric solid elements were used to model the deck, the folded plate, the end diaphragms, the gusset plates and the anchors for the post-tensioning tendons. The diagonals and the post-tensioning tendons were idealized as three dimensional truss elements (STIFF 8 ANSYS element library). A sensitivity analysis was performed to determine the most economical size of solid elements to use in the model. There were two quantities investigated in the sensitivity analysis-the height to width ratio and the width to length ratio. For the deck elements, the length of the element was measured in the global X-direction (longitudinal direction), the width was measured in the global Y-direction (transverse direction) and the height in the global Z-direction (vertical direction). Initially, a sensitivity analysis was performed by analyzing a 6 in. thick simply supported slab of 8 ft. span (see Figure 4.2 and Table 2).

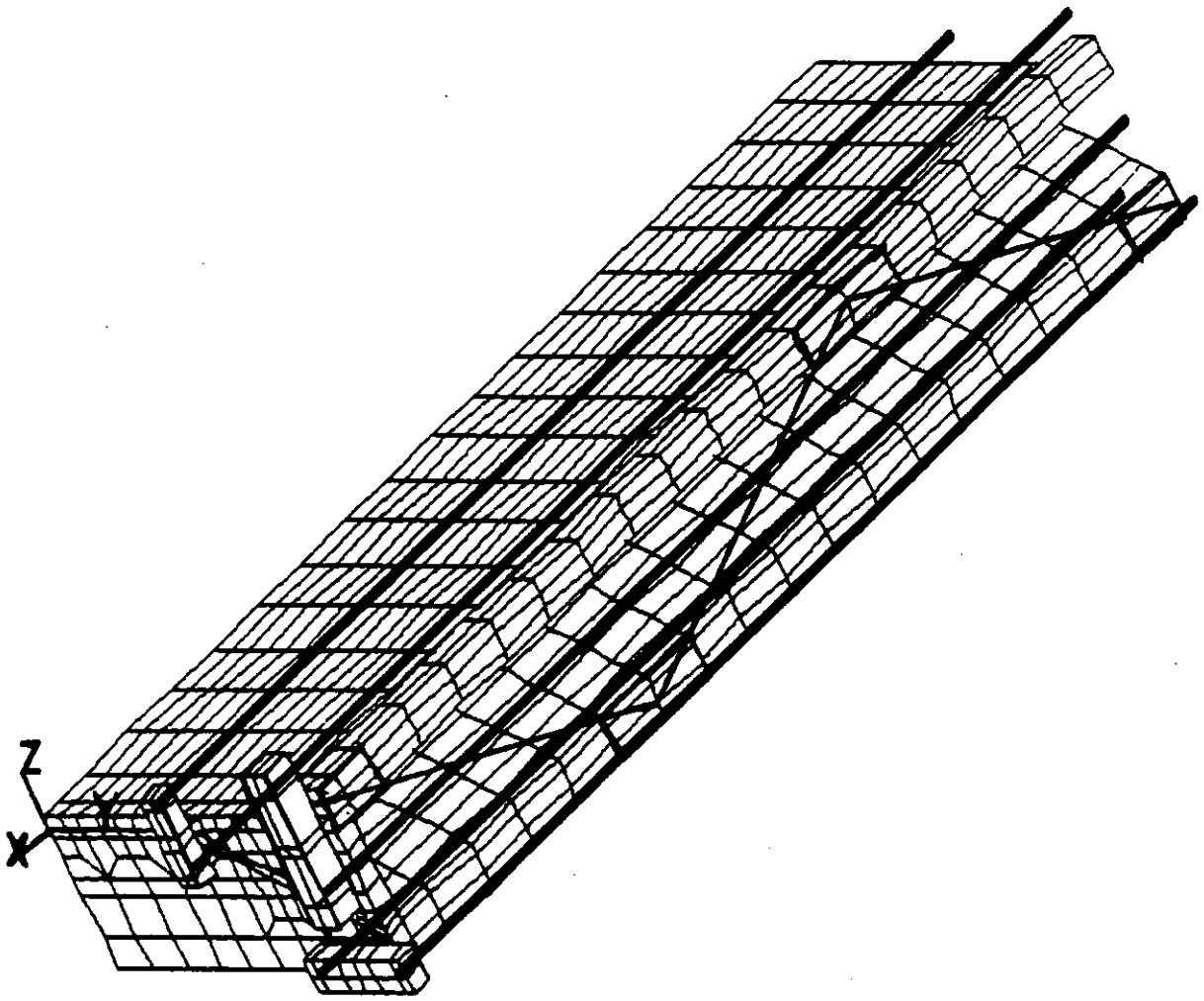

(a) Perspective view

Figure 4.1. Finite element model for integrated deck and folded plate bridge structure

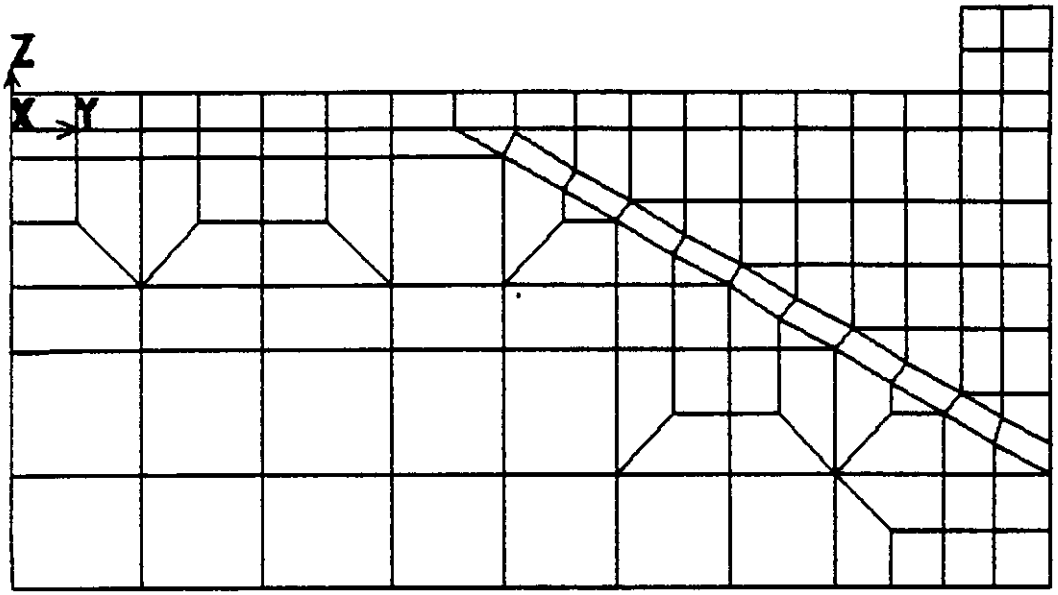

(b) Finite element mesh for diaphragm

Figure 4.1. (continued)

In this analysis, the length of the elements was kept constant and the height to width ratio was varied from 1:1 to 1:4. The results of these analyses are presented in Table 2. One can observe that slabs modelled using solid elements having a height to width ratio of less than 1:2 give satisfactory results compared to results from simple statics. To obtain better results, all the elements in the bridge deck and the inclined plates were required to have equal width; therefore to facilitate the modelling of the deck with approximately equal size elements, 1:1.7 was the average height to width ratio adopted.

In the second part of the sensitivity analysis, a 6 in. thick simply supported slab of 48 ft. span was analyzed (see Figure 4.3). Here the width of the element was kept constant, the height to width ratio maintained at 1:2 and the width to length ratio varied from 1:2 to 1:6. The results of this analysis are shown in Table 3. Initially, the length of all elements measured in the global X-direction was not equal, as nodes were located according to the size and position of the gusset plates (see Figure 4.4a). Thus, the finite element model was similar to the actual scaled Plexiglass model. However, these variations in the length of the elements caused sharp unlikely variations in the longitudinal stress in the deck. Therefore, the length of all elements was made uniform as shown in Figure 4.4b. With this modification the gusset plates had to be modelled slightly smaller or larger than their actual size. This small discrepancy in the modelling of the gusset plates however did result in a continuous, smooth, longitudinal stress variation in the global X-direction. It can be observed from Table 3 that even with a width to length ratio of 1:6 sufficiently accurate results could be obtained, however a smaller and

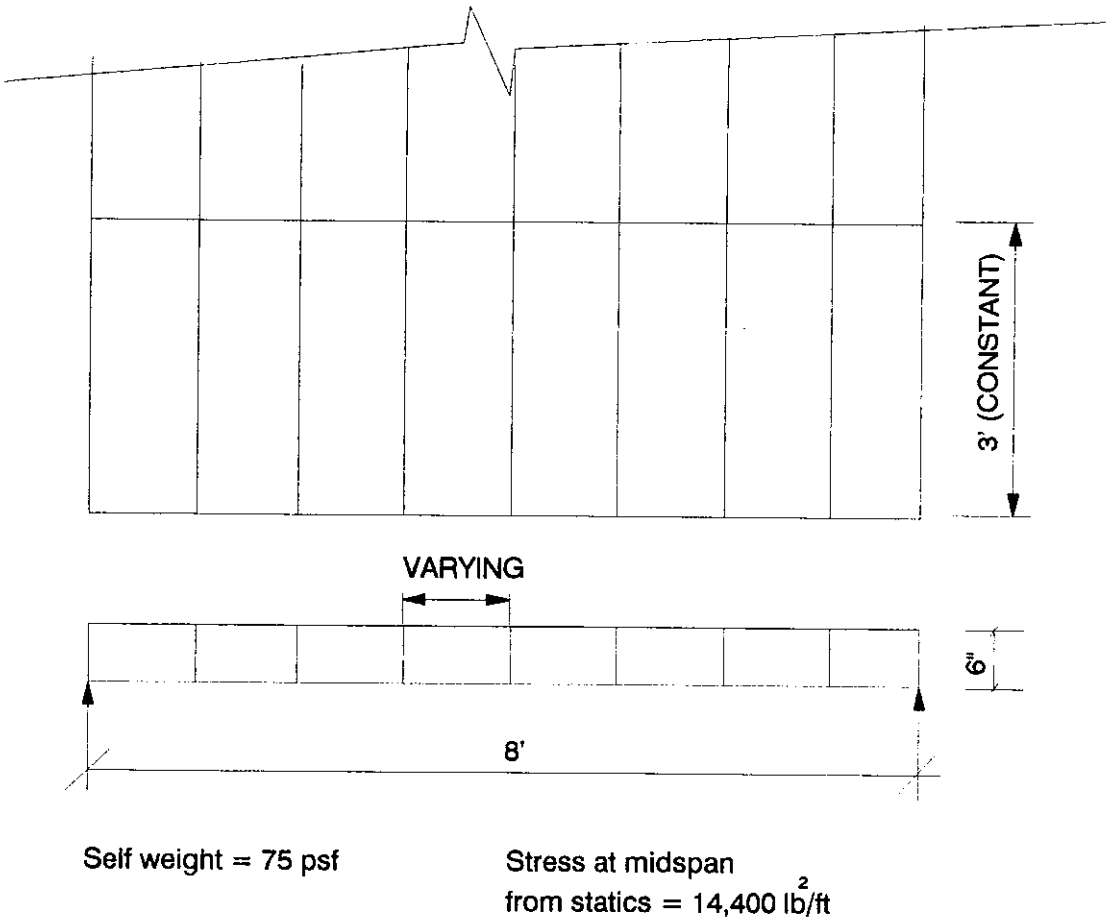

Figure 4.2. Finite element model of a slab for studying the effect of height to width raio of three dimensional isoparametric solid elements

Table 2. Results of sensitivity study for height to width ratio of solid elements compared to results from static analysis (see Figure 4.2).

Height to Width ratio	Stress at midspan	% Error
1:1	14,000	2.80
1:2	13,700	4.90
1:2.67	13,300	7.60
1:4	12,400	13.90

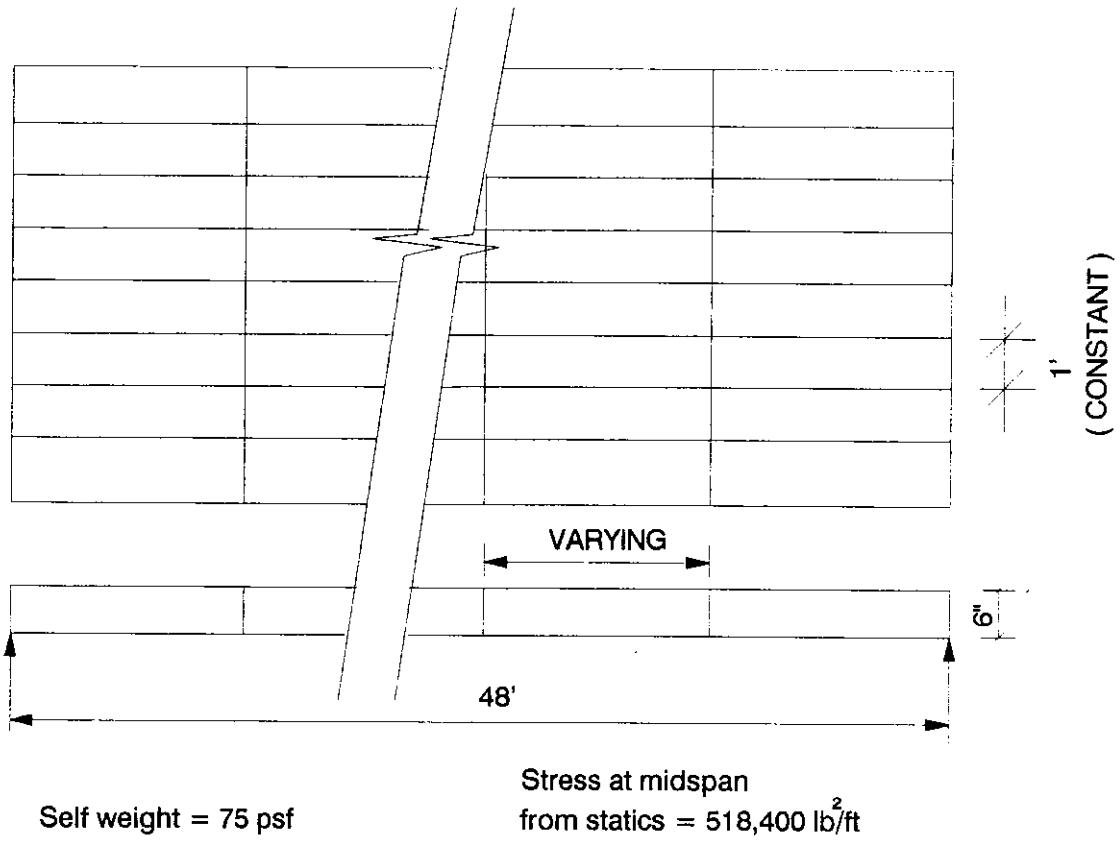

Figure 4.3. Finite element model of a slab for studying the effect of width to length ratio of three dimensional isoparametric solid elements

Table 3. Results of sensitivity study for width to length ratio of solid elements compared to results from static analysis (see Figure 4.3).

Width to Length ratio	Stress at midspan	% Error
1:2	516,800	0.30
1:3	514,200	0.80
1:4	510,500	1.50
1:6	499,900	3.60

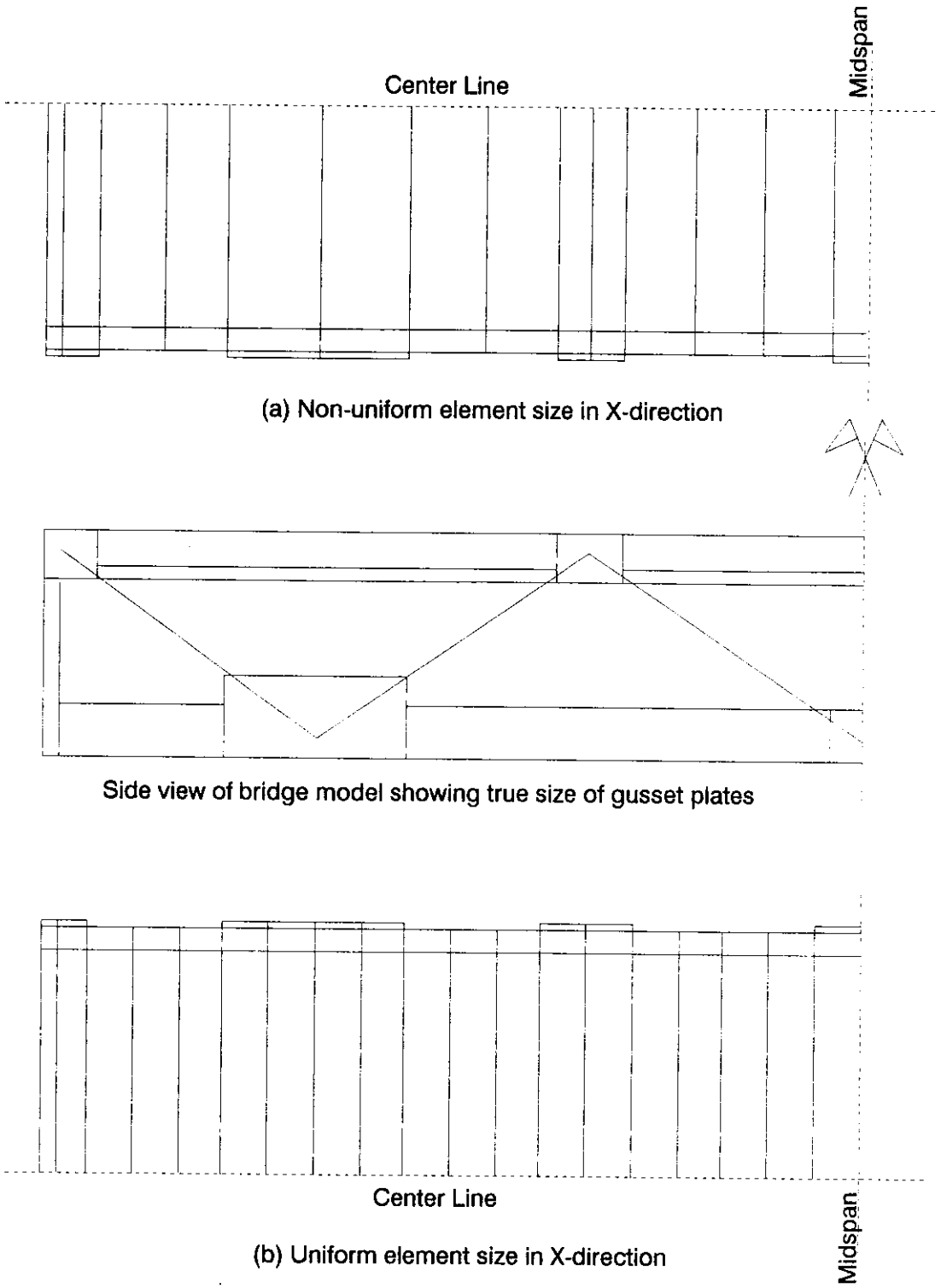

Figure 4.4. Plan view of finite element model with uniform and non-uniform element size in the X-direction

better width to length ratio of 1:3 was adopted so that the inaccuracy in modelling the size of the gusset plates was not as significant.

Generally, an 8 node isoparametric solid element is not an ideal choice for modelling a structure which is predominantly experiencing flexural action because, it is a linear element and only linear deformation can be obtained along its edge. However, ANSYS gives the user an option to include modified extra displacement shapes. Inclusion of the extra displacement shapes allows higher order displacement effects to be characterized with fewer elements. This feature made the use of three dimensional isoparametric solid elements practical for the modelling of the integrated deck and folded plate bridge structure.

4.3. Prestressing of finite element model

Prestressing force can be modelled by applying an initial strain to the post-tensioning tendons which are modelled using three dimensional spar elements. A positive initial strain in the tendons creates a tensile force in the tendons which acts as the prestressing force on the bridge. Another method to simulate the prestressing force is to apply element pressures equivalent to the required prestressing force on respective element faces at the diaphragm end of the bridge. In this second method post-tensioning tendons are not required but the prestressing force remains constant under loading. However, in the Plexiglass model when load is applied, the bridge deflects and the prestressing force changes. Hence, to simulate the change in the prestressing force along

with the deformation of the bridge, the first method of modelling the prestressing force using the spar elements was adopted.

Simulating the scaled model, the arrangement for prestressing the finite element model consisted of 2 aluminum tendons for the deck in each half of the bridge, 2 steel tendons at each curb and 2 steel tendons for each bottom beam as shown in Figure 4.1a. As determined earlier in Section 2.5, each tendon in the deck and the curb was required to apply a force of 30.625 lb and each tendon in the bottom beam was required to apply a 93 lb force. To apply these forces the average required strains were 111×10^{-6} in/in, 37×10^{-6} in/in and 112×10^{-6} in/in for the tendons prestressing the deck, the curb and the bottom beam, respectively. While post-tensioning any structure, as the post-tensioning force increases it is accompanied by the instantaneous axial shortening and bending of the structure. This results in loss of strain in the post-tensioning tendons, thus reducing the post-tensioning force. In actual practice, it is easy to overcome this by monitoring the net strain in the tendons after the instantaneous losses have occurred. Similarly, due to axial shortening and bending of the finite element model, there will be some loss in the specified initial strains of the post-tensioning tendons. However, the loss of prestressing force in the finite element model can be detected only after the execution of an analysis. Hence, the analysis was executed with only the prestressing force (which is modelled by specifying initial strain in the tendons) as load on the model. Resulting strains in the tendons after the analysis was completed were monitored. The initial strains were then adjusted such that the resulting strains in the tendons after the losses had occurred were equal to the required strains, so that the model experiences the

required prestressing force. Table 4 shows the initial strain values which had to be specified and the resulting strains in the tendons after the analysis was completed. One can observe that the averages of resulting strains in each pair of tendons are approximately equal to the required strains, however the difference between the initial and resulting strains varied depending on the location of the tendons. To check that the method of modelling the prestressing force produced the correct stresses, the longitudinal stresses in the bridge deck caused by both the above mentioned prestressing arrangements were compared and observed to be in good agreement, thus validating the modelling of the prestressing force.

Table 4. Initial strains and resulting strains in the three dimensional spar elements used to model the post-tensioning tendons of the bridge

Tendon material	Tendon position	Initial strain (MII)	Resulting strain (MII)	Average of resulting strain in pair of tendons (MII)
Aluminum	Top of Deck	167	114	112
	Bottom of Deck	243	110	
Steel	Top of Curb	60	41.4	37.9
	Bottom of Curb	210	34.3	
Steel	Inside of Beam	536	111	112
	Outside of Beam	522	112	

5. TESTING AND ANALYSIS OF RESULTS

5.1. Test Procedure

The Plexiglass bridge model was tested using a single concentrated load placed at several predetermined locations on the deck at the intersection of the longitudinal and transverse axes shown in Figure 5.1. Response of the model was studied by monitoring the deflections and strains in the model. A load of 7.5 lb, which is approximately equal to the scaled load on one trailer axle of a standard HS20-44 truck [1] was used in testing. This loading was adequate to produce strains of sufficient magnitude in the vicinity of the load so that they could be accurately measured. The weight used to apply the 7.5 lb load was placed on a small rubber pad of dimension 0.75 in.x 0.75 in.x 0.5 in. to concentrate the load over a small area.The model was tested once with 6 diagonals and once without any diagonals connecting the edge beams and the curbs as shown in Figure 5.2. For testing the model without prestressing force, the following steps were followed:

- Position the rubber pad over the point to be loaded.
- Power the strain gages and wait for approximately 30 seconds to allow the gage temperatures to stabilize.
- Initialize the strain gages.
- Place the 7.5 lb load on the rubber pad and immediately read the gages.
- Shut off the power to the gages, remove the load and wait for at least 10 minutes before repeating the procedure for another load position.

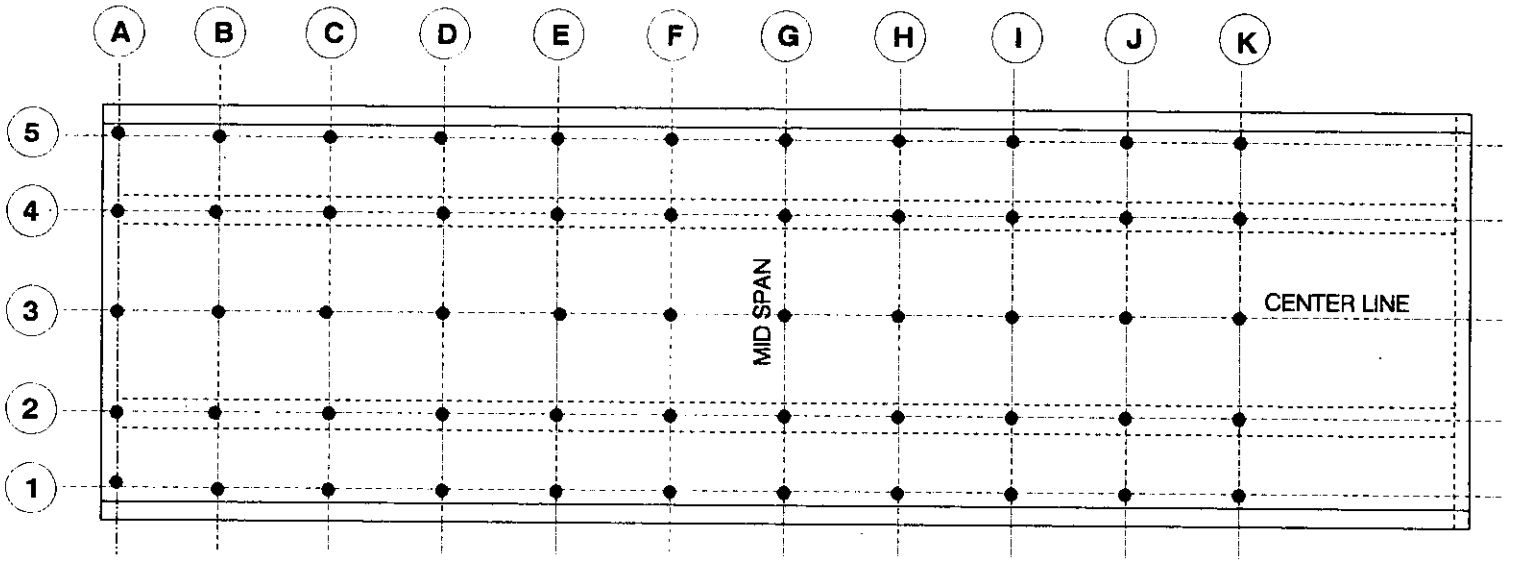

Figure 5.1. Load point locations for a single concentrated load

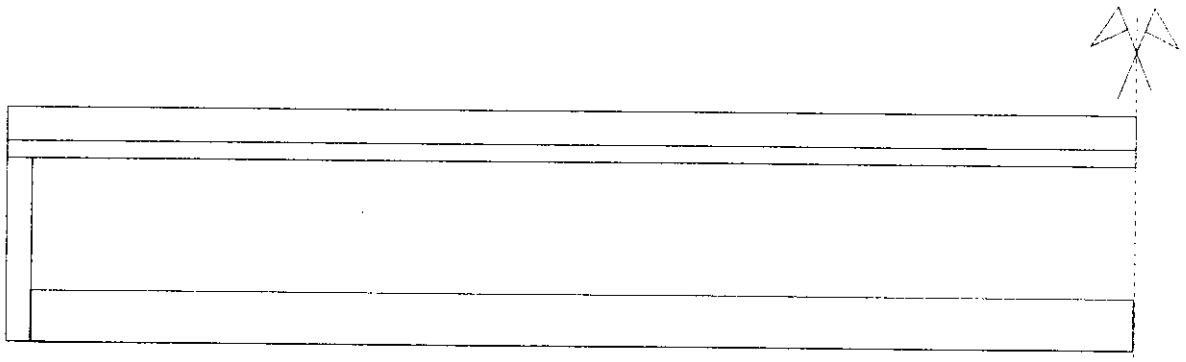

(a) CONFIGURATION 1: MODEL WITHOUT DIAGONAL MEMBERS

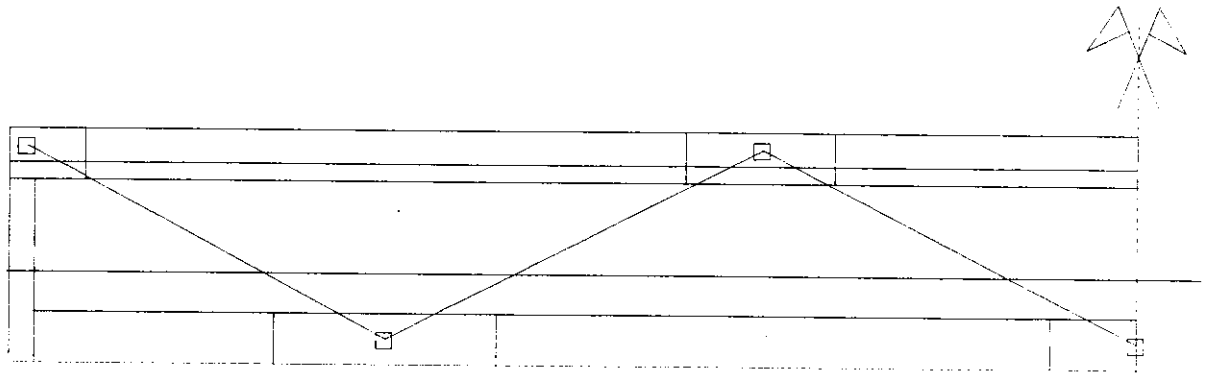

(b) CONFIGURATION 2: MODEL WITH 6 DIAGONAL MEMBERS

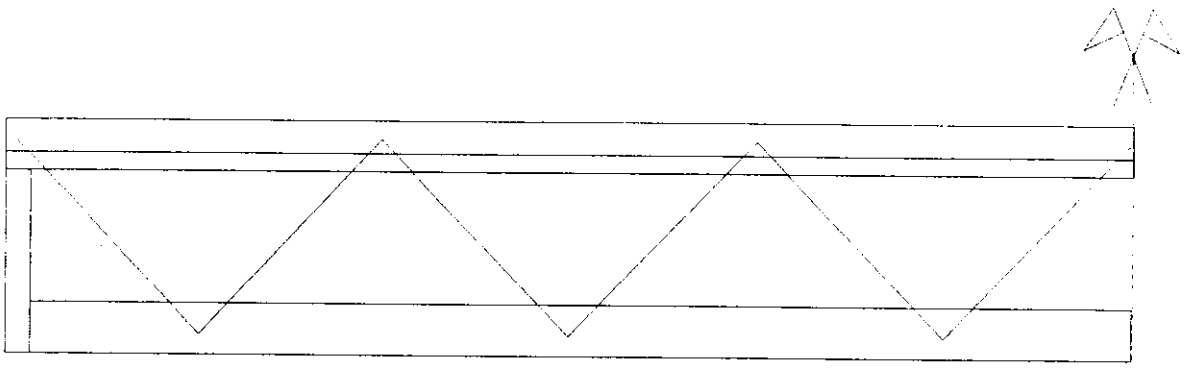

(c) CONFIGURATION 3: MODEL WITH 12 DIAGONAL MEMBERS

(ONLY FOR FINITE ELEMENT ANALYSIS)

Figure 5.2. Side view of model showing different web member configurations

As soon as power was turned on, the initial surge of current in the strain gages raised the gage temperature which affected the strain readings. The gage temperatures were observed to stabilize in approximately 30 seconds after which the strain readings also stabilized; hence each time the power was turned on, a little time was allowed to elapse before initializing or reading strain gages. Also, even though the model was loaded for a very short period of time for each load case, a 10 minute interval was observed between two consecutive load tests to allow for creep recovery in Plexiglass. Once the load had been removed, it was observed that a 10 minute interval was sufficient to allow the strains in the model to return to zero. Using the above procedure, power was supplied to the gages for less than two minutes and the time lag between initializing and reading the gages was minimized, thus limiting the drift in the gages.

When prestressing force was applied to the model the following testing procedure was used:

- Power the strain gages and wait for approximately 30 seconds.
- Initialize all the gages and shut off the power to the gages.
- Apply tension to the post-tensioning tendons and read the strains in the tendons only.
- Adjust force in the tendons until the desired force is obtained.
- Place the 7.5 lb load at the desired position and immediately read the strains in the bridge model.
- Remove the load,wait for at least 10 minutes, reposition the load and read strains for new load position.

5.2. Test results and discussion: no prestressing force

This section presents the response of the model under a single concentrated load. Test results and analytical results from a finite element analysis are presented for tests on the model having no diagonals and 6 diagonals connecting the curbs and the edge beams. To document the effect of connecting the curb and the beam by diagonal truss members, analytical results from a finite element model with 12 diagonals are also presented.

5.2.1. Response of the deck

Figure 5.3 compares the deflection of the deck at midspan when the single concentrated load is placed at position G1 for the model with no diagonals and 12 diagonals connecting the curb and beam. The difference between the finite element results and the experimental results for the deflection across the deck at midspan was within 13%, see Figure 5.3. The deck behaves like a plate supported on four elastic supports, along the curbs and along the connections of the deck and the inclined plates. Stiffness of the curbs alone is small, hence when there are no diagonals connecting the curbs and the beams, the deck beyond the connection with the inclined plates behaves more like a cantilevered plate. However when the curbs and the beams are connected by diagonal members, they form a truss and provide stiff supports to the edge of the deck. The addition of the truss members reduces the overall deflection of the deck and results in higher torsional stiffness as indicated by the smaller differential displacement between the edges A and C of the deck as shown in Figure 5.3.

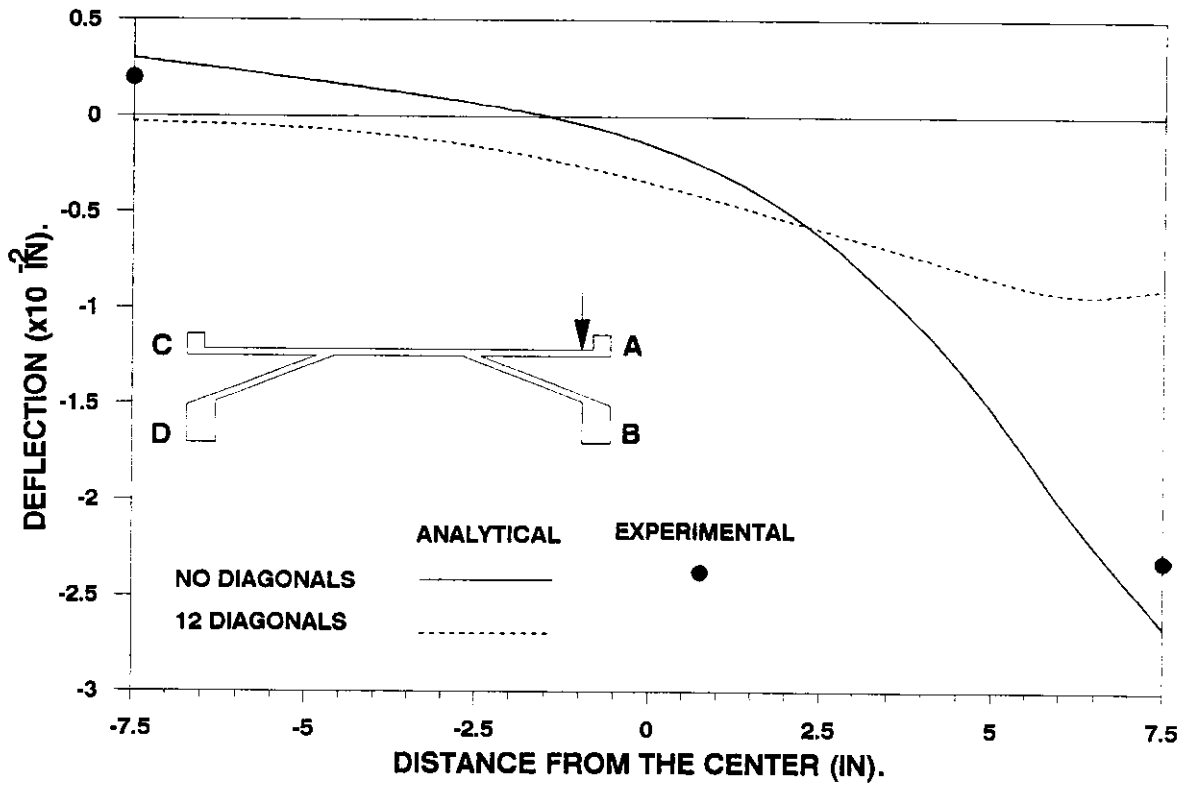

Figure 5.3. Deflection across the deck at midspan, single load at position G1

The transverse strain in the top of the deck at midspan when the load is placed at positions G1 and G3 is shown in Figures 5.4a and 5.4b, respectively. As can be seen from Figures 5.4a and 5.4b the experimental and finite element results are in very good agreement. The tensile transverse strains in the top of the deck when load is at position G1 reduce with the addition of 6 diagonals and they reduce greatly when 12 diagonals are present (see Figure 5.4a). Evidently 6 diagonals do not significantly increase the stiffness of the curb. This also reinforces the assumption that the deck in the absence of the diagonals acts more like a plate with double cantilevers and in the presence of the diagonals the edge supports of the deck are stiffened and the deck acts like a plate on four elastic supports. As shown in Figure 5.4b, when the load is moved to the center of the deck (load at G3) the transverse strains in the deck become essentially independent of the diagonal members. Thus it can be concluded that connecting the curb to the beam has more effect on improving the structural behavior of the section under load applied near the curbs than under load applied near the center of the deck.

The bridge deck has a shorter span in the transverse direction, hence the behavior of the deck near midspan, far from the end diaphragms is more like a continuous one way slab in the transverse direction and the strains in the longitudinal direction are small. Except, in the vicinity of the concentrated load, the strains are very high due to local distortions near the point of loading (see Figures 5.5 and 5.6). Figure 5.5 shows the distribution of the longitudinal strain across the top of the deck at midspan for two different load positions. As can be observed, the longitudinal strain in the deck is not significantly effected by the presence of the diagonals connecting the curbs to the edge beams. The

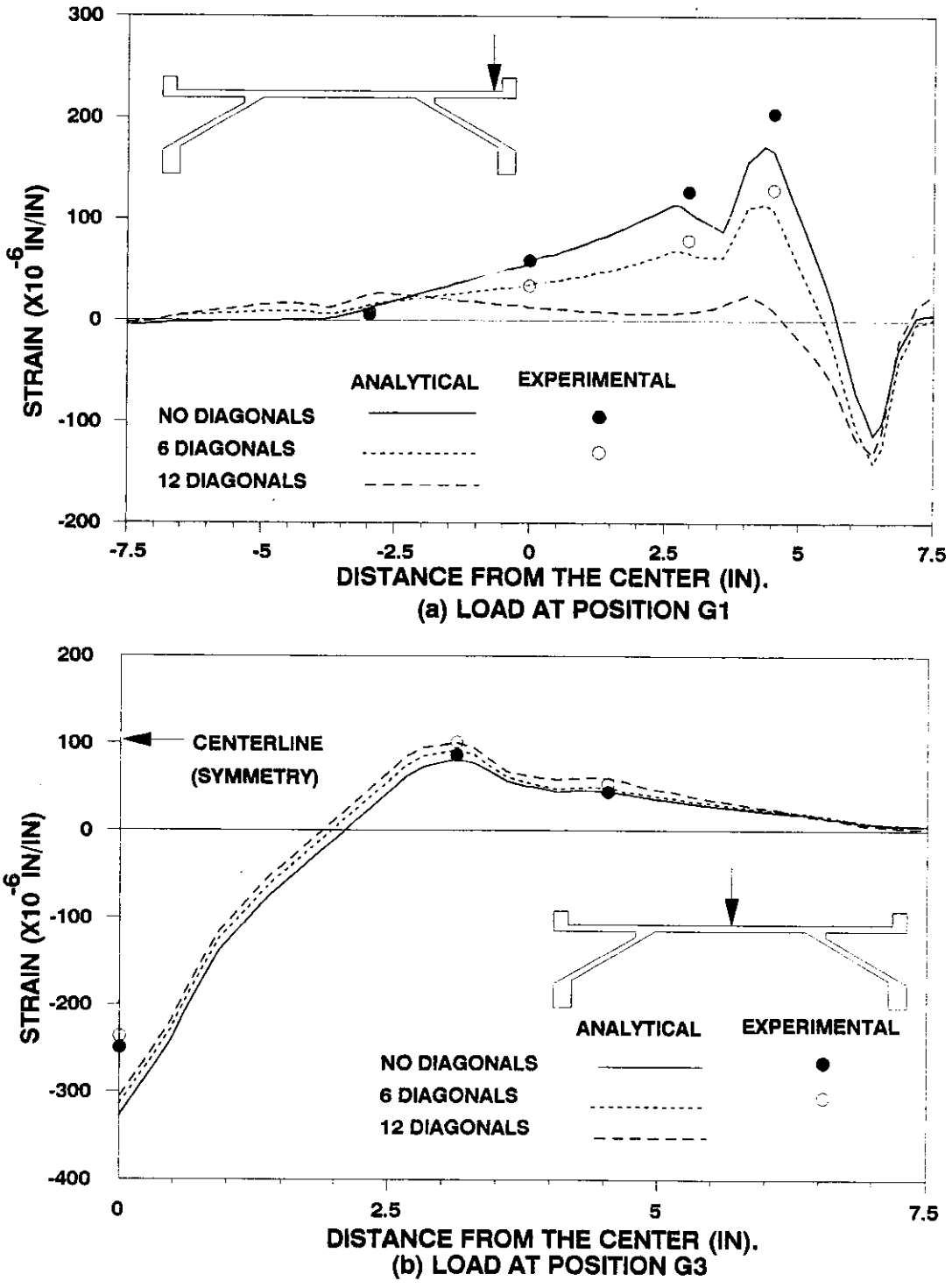

Figure 5.4. Transverse strain distribution on top of the deck at midspan : single load at positions G1 and G3

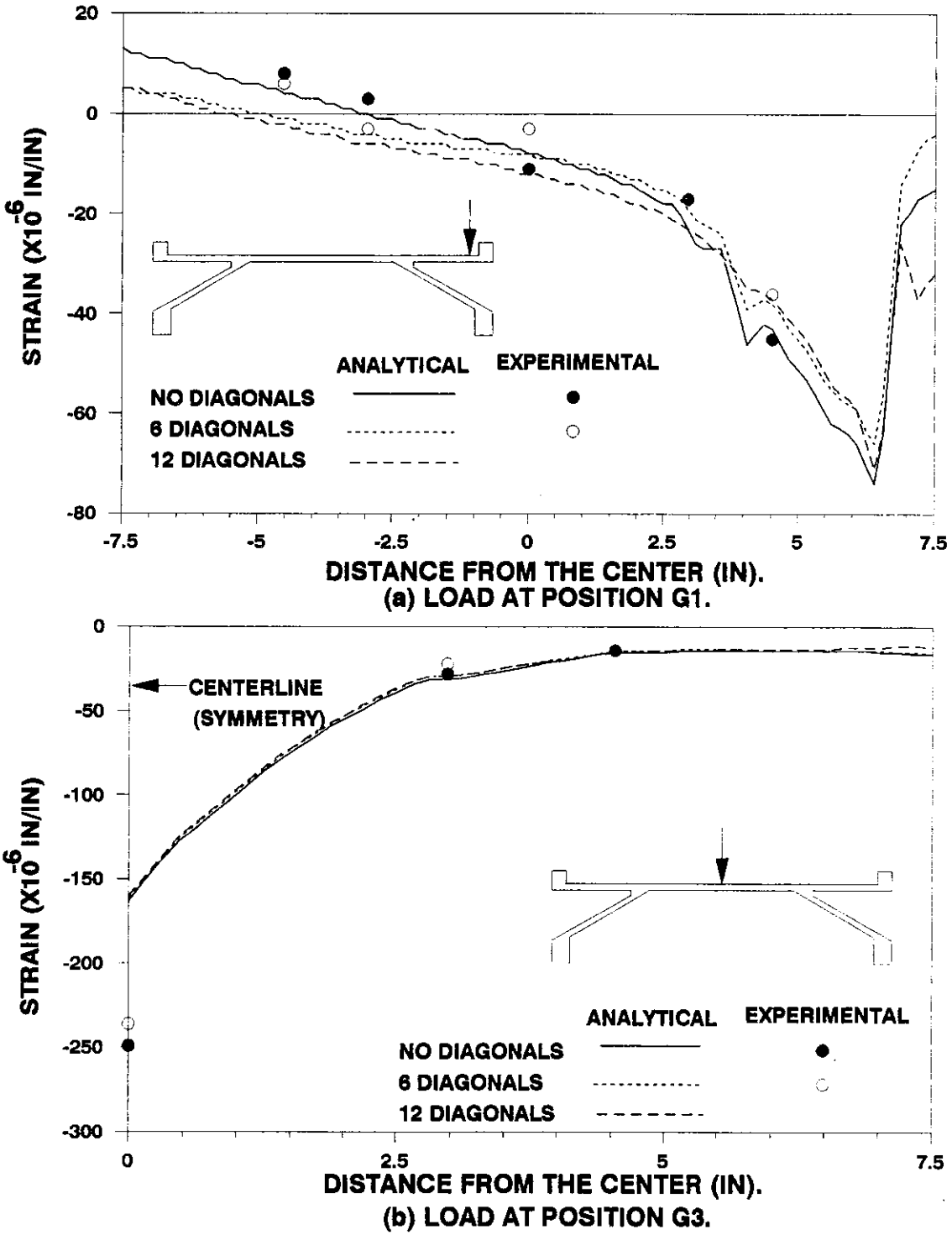

Figure 5.5. Longitudinal strain distribution on top of the deck at midspan : single load at positions G1 and G3

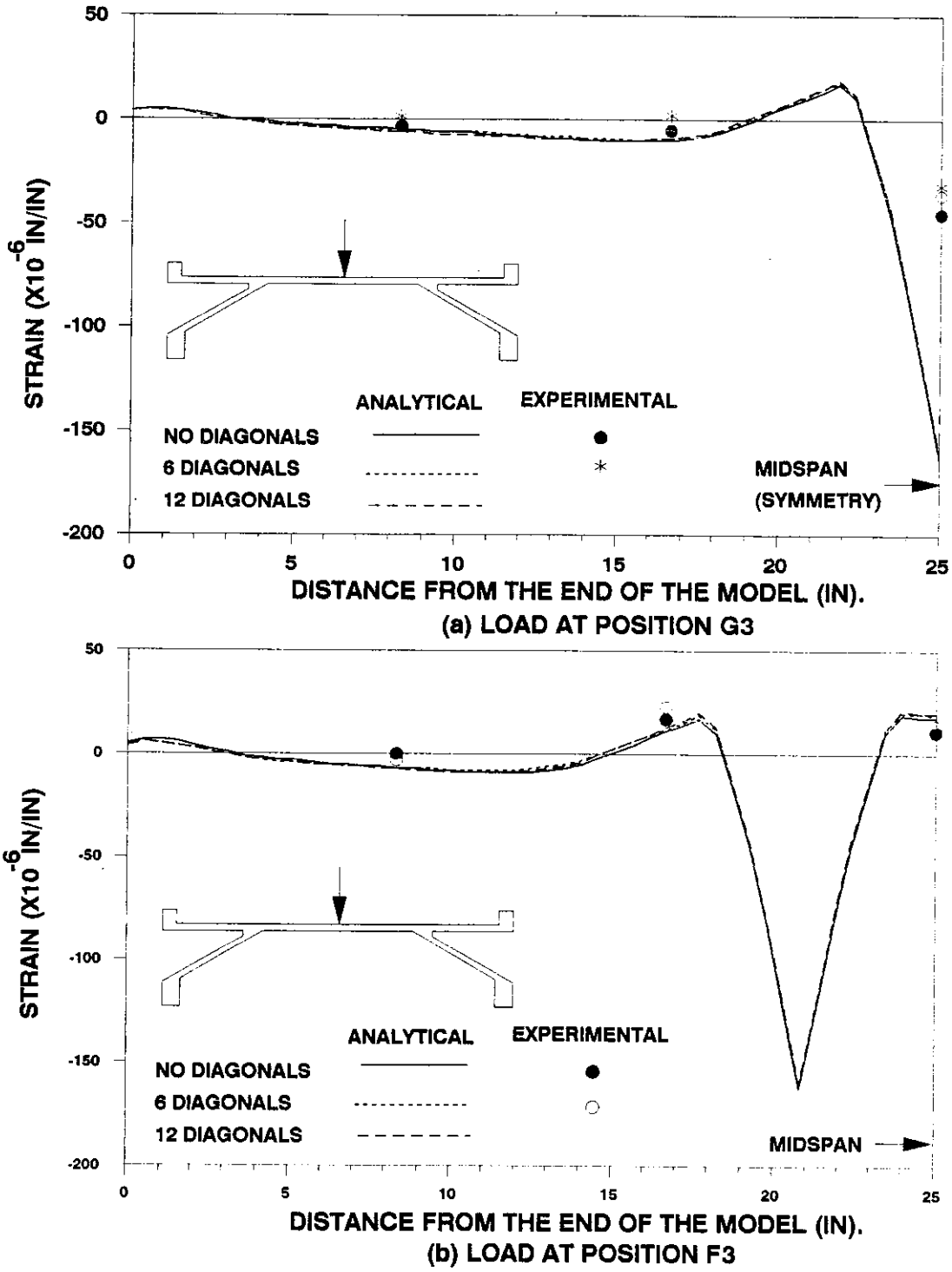

Figure 5.6. Longitudinal strain distribution on top of the deck along center line of the deck: single load at positions G3 and F3

longitudinal strain in the top of the deck and along the center line of the deck (i.e. along section 3) is shown in Figure 5.6 for two load positions. The experimental and analytical results agree well overall, but differ significantly at the point of loading as is prominently seen in Figure 5.6a. There are two probable reasons for the difference in the analytical and experimental results at the point of loading:

i) The load in the finite element analysis is a true point load, where as the load in the experimental testing is applied on an area 0.75 in.x 0.75 in.

ii) From the finite element analysis, the strain exactly under the point load was calculated, but during experimental testing the load could not be placed directly on the strain gage and was placed near it. Strain recorded close to the load was taken as the strain under the load.

One has to be careful while interpreting the results shown in Figure 5.6 as they are affected by the high value of Poisson's ratio for Plexiglass. The shorter "span" being in the transverse direction, the main load transfer in the deck is in the transverse direction resulting in compressive strains in the top of the deck in the transverse direction. These compressive strains in the transverse direction produce tensile strains in the longitudinal direction (see Figure 5.6) due to the Poisson's ratio effect. These tensile longitudinal strains may not be present in a concrete prototype since the Poisson's ratio of concrete is approximately half that of Plexiglass.

5.2.2. Response of the curbs and the beams

Longitudinal strains along the top of curb A and the bottom of edge beam B when the load is at position G1 are shown in Figures 5.7a and 5.7b,

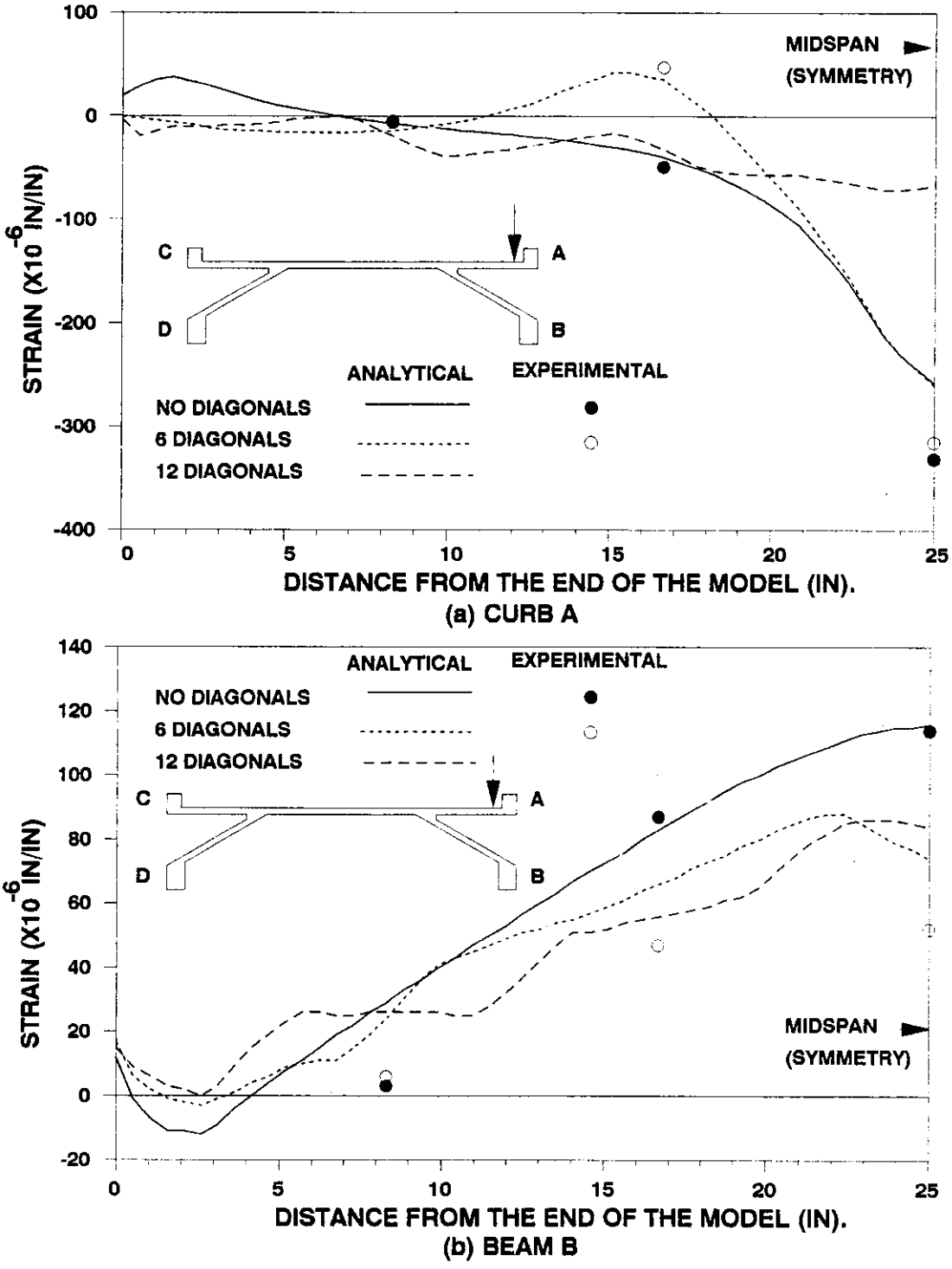

Figure 5.7. Longitudinal strain distribution along top of the curb A and bottom of beam B: single load at position G1

respectively. As can be seen from Figure 5.7a, the strain in the top of the curb is greatly reduced when 12 diagonals are used to connect the curbs and the edge beams. The curve of longitudinal strain in the top of the curb for model with 6 diagonals indicates the curb behaves like a continuous beam supported at points where two diagonal truss members meet at the curb. Connecting the curbs and the beams with only 6 diagonals does not reduce the strains in the curb. For the curb to behave more like a truss element and reduce the flexural bending of the curb, more diagonal truss elements are required. The advantage of adding more diagonal members is clearly reflected in Figure 5.7a. When one observes the longitudinal strain in the beam (see Figure 5.7b), the presence of 6 diagonals reduces the longitudinal strain in the edge beam by approximately 33%. However increasing the number of diagonals from 6 to 12 does not significantly effect the strain in the edge beam. Comparing the experimental and finite element results in Figure 5.7 one observes better agreement when there are no diagonals; the agreement between the two is not as good when the diagonals are present. This may be caused by the discrepancy in the modelling of the gusset plates as noted in Section 4.2.

Figures 5.8 and 5.9 show the symmetric response of the model. Figure 5.8a shows the change in the longitudinal strain in the top of the curbs A and C at midspan as the load moves across the deck along section G at midspan. Apart from the symmetric response, it can again be observed that the strain in the top of the curb was not significantly affected when 6 diagonals were used to connect the beams and the curbs. Similarly Figure 5.8b shows the change in the longitudinal strain in the bottom of the beam at midspan as the load moves across section G. In this case, the significant reduction in strain can be

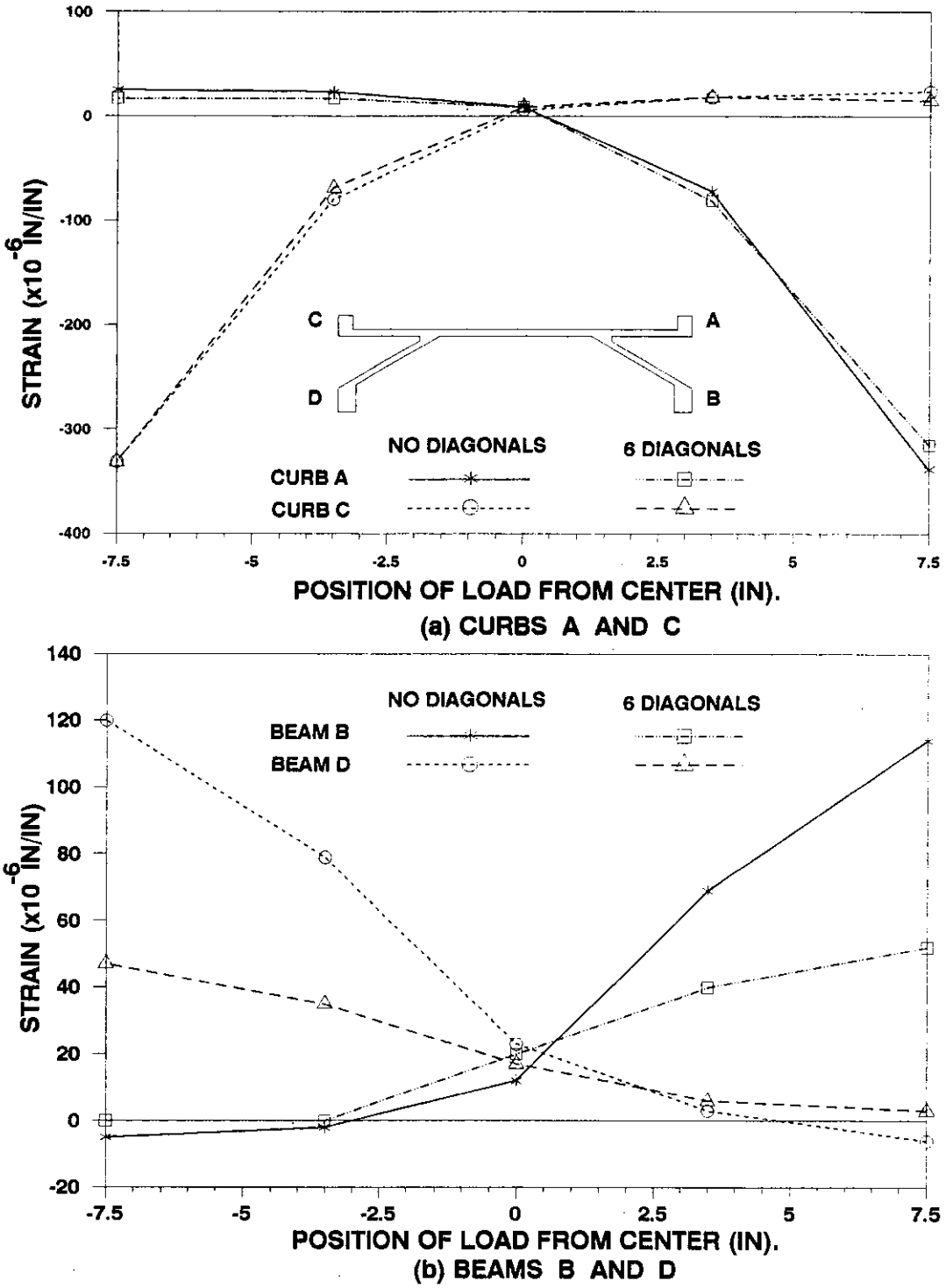

Figure 5.8. Longitudinal strain at midspan in top of the curbs and bottom of the beams caused by a single load moving across section G

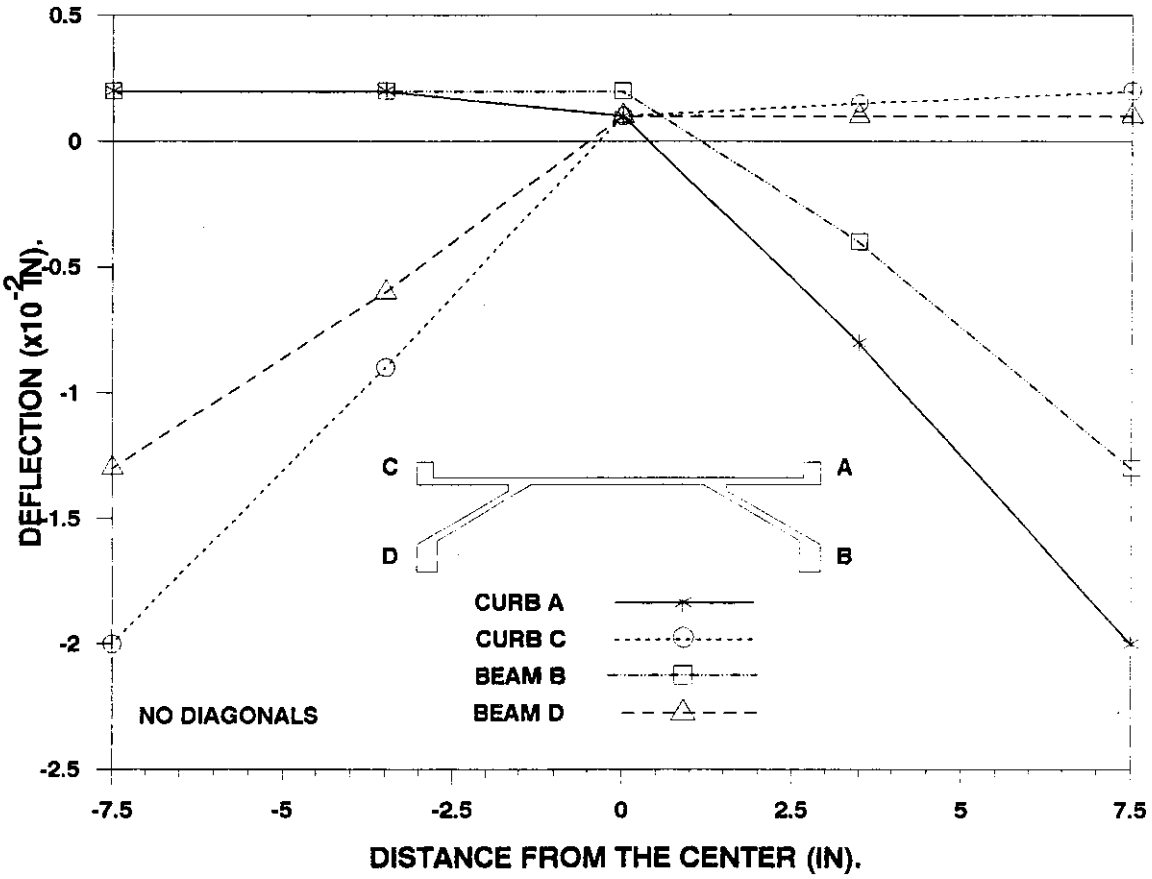

Figure 5.9. Deflection of the curbs and the beams at midspan due to a single load moving along section G at midspan

observed when 6 diagonals are used to connect the curb and the beam. Figure 5.9 shows the deflection of the curbs and the beams at midspan for the model with no diagonals as the load moves across section G. For loads near the curb, the deflection of the curb is much greater than that of the beam when there are no diagonals. Connecting the curb and the beam minimizes the differential deflection between the curb and the beam and force the entire cross section to act as one unit which obviously results in a stiffer section. Reviewing Figures 5.8 and 5.9, one can conclude that the strain and deflection yield similar information regarding the behavior of the structure.

5.2.3. Response of the inclined plates

As the concentrated load moves across the deck along section G, the effect on the longitudinal and transverse strains at midspan at position P in the inclined plates is shown in Figure 5.10. The longitudinal strain in the inclined plate at midspan was not significantly affected by the addition of diagonals as shown in Figure 5.10a. The longitudinal strain decreased as the load moved from the right side of the bridge (position G1) to the left (position G5). As previously stated, the presence of the diagonals increases the torsional rigidity of the bridge section and reduces the rotation at the joint between the deck and the inclined plate; this reduces the transverse strains in the inclined plate when the load is at G1 (see Figure 5.10b). From Figure 5.10b it can also be observed that the transverse strains were larger when the load was at positions G1 and G3 since load at these positions caused more rotation of the joint between the deck and the inclined plate. The transverse strain at point P in the inclined plate becomes negligible as the load moves towards position G5.

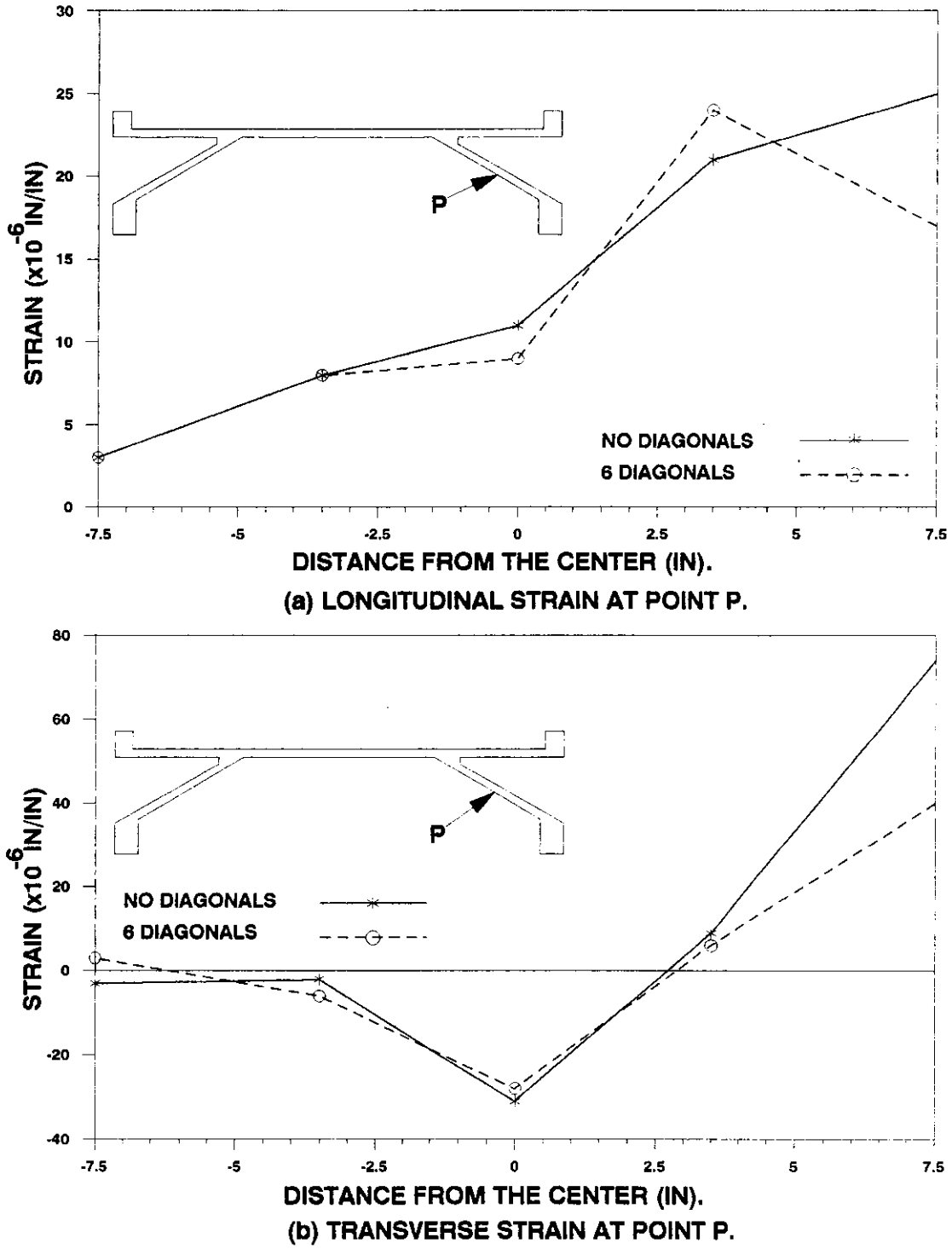

Figure 5.10. Longitudinal and transverse strain at position P at midspan in bottom of the inclined plates: single load moving along section G

The shear stresses in the bottom of the inclined plates were computed using the strain readings in the rosettes mounted on the bottom of these plates near the end diaphragms (see Figure 3.2). The calculations showed that the shear stress was maximum when the concentrated load was at position B2. In this loading case, most of the load is transferred to the support through the inclined plates resulting in higher shear stresses in the inclined plates near the diaphragm. Figure 5.11 shows the shear stresses in the bottom of the inclined plate very near the end diaphragm for load at B2. The shear stress is almost uniform in the plate except the regions where the plate is joined to the deck and to the beam. Diagonals (in place or removed) had no significant effect on the shear stresses in the end plates. Shear stresses computed from experimentally recorded strains agree closely with the stresses obtained from the finite element analysis (see Figure 5.11). However significant errors can be introduced in recording the shear strains using three separate gages to form a rosette (see Figure 3.2), as all the gages are recording strains at slightly different points and the angle between them cannot be accurately controlled when the gages are mounted.

5.3. Test results and discussion: prestressing force applied

Prestressing the Plexiglass model was not an easy task. Adjusting the force in the tendons to the desired magnitude took a very long time because of the high creep of Plexiglass. The strain in the tendons was continuously decreasing due to the creep of the Plexiglass. This resulted in a loss of prestressing force which had to be compensated by applying more tension to the tendons. Finally as the rate of creep reduced, the force in the tendons

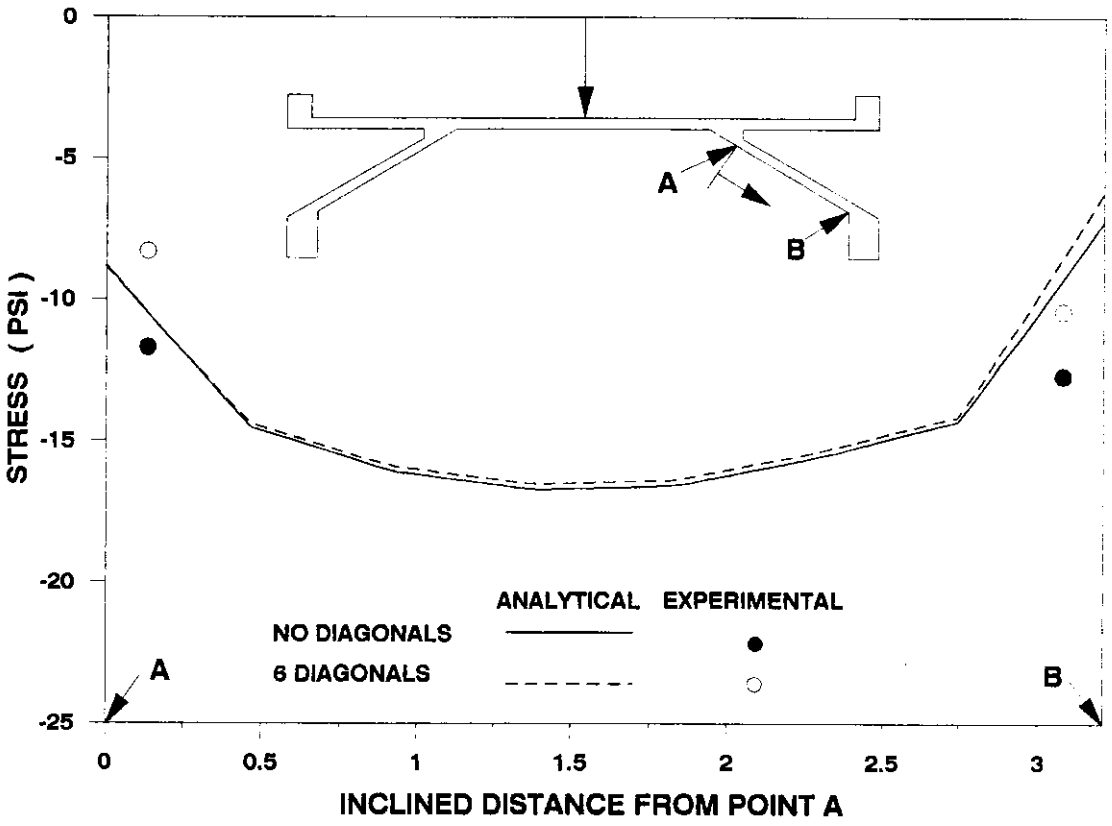

Figure 5.11. Shear stress distribution on bottom of the inclined plates near the diaphragm: single load at position B2

stabilized. However, while the post-tensioning force in the tendons was being adjusted, the strains in the Plexiglass model induced by the post-tensioning force had been accumulating due to creep of Plexiglass. Creep of Plexiglass can not easily be incorporated in the finite element analysis of the model. Hence, the experimental and analytical results do not agree when the prestressing force was applied. Figures 5.12a and 5.12b show the longitudinal strain in the edge beam and along the center line of the deck due to applied post-tensioning forces alone. The difference in the experimental and the analytical results reflect the effect of accumulation of creep strain in Plexiglass. Since post-tensioning force is directly applied to the edge beam, the creep strain is more in the edge beam (Figure 5.12a) than along the center line of the deck (Figure 5.12b). Thus, the disagreement between the experimental and analytical results is more in Figure 5.12a (bottom of beam) than in Figure 5.12b (along section 3). A constant prestressing force could not be maintained in the Plexiglass model due to creep of Plexiglass, which also made it difficult to reproduce the experimental test results. Hence, the experimental results when prestressing force was applied were unreliable, thus additional experimental data for model with prestressing force are not presented. If practically possible, a better method of prestressing a Plexiglass model could be one which produces constant strain in the model rather than the present method which applies a constant prestress.

5.4. Response of the model under truck loading: prestressing force applied

After studying the response of the structure under a single concentrated load and verifying the results of the finite element analysis, the structure was

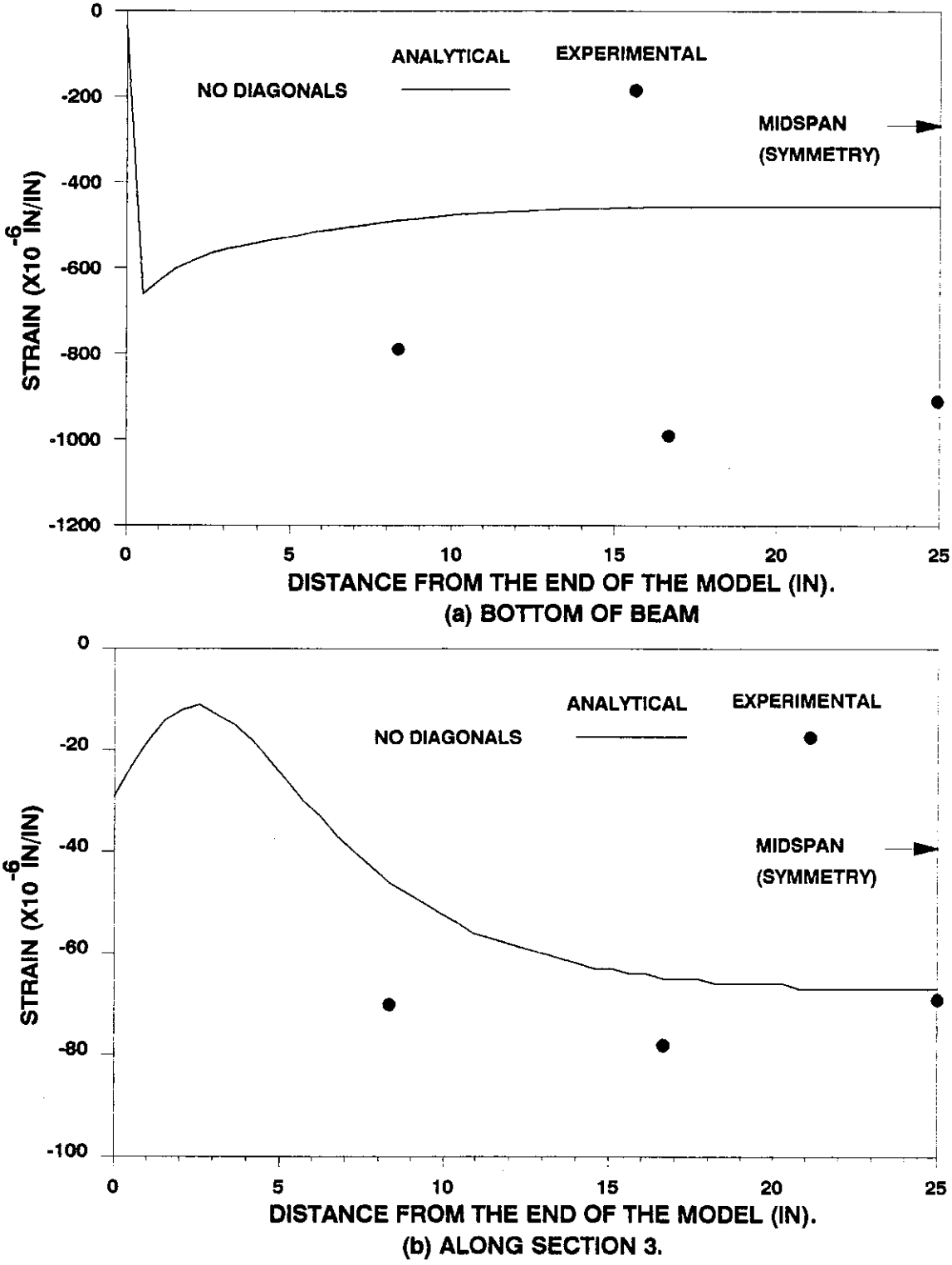

Figure 5.12. Longitudinal strain distribution due to only prestressing forces in bottom of the beam and in top of deck along center line (along section 3)

subjected to post-tensioning forces (determined in Section 2.5), dead and live loads and analyzed using the finite element method. Two configurations were analyzed, one with no diagonals and one with 12 diagonals connecting the curbs and the beams. The live load applied was equivalent to the HS20-44 truck loading specifications of AASHTO [1]. To save computation time, the truck loading of AASHTO was modified according to Andrey [3] so that a quarter symmetry can be used in the finite element analysis. The modification of truck loads was accomplished in two steps; first, the scaled distances between the axles of the actual truck were taken to be 6.94 in. so that the wheel load coincides with a nodal point location in the finite element model. Secondly, a modified truck load that predicts the same bending moment in a simply supported beam as the actual truck load was evaluated. The actual truck load as defined by AASHTO, the truck loading scaled for the model and the modified truck load are shown in Figure 5.13. The trucks were placed at midspan as close to the curb as permitted by AASHTO [1] to obtain the maximum bending moment in the structure at midspan.

Longitudinal strain under dead and live loads along with the applied prestressing force in the top of the curb and the bottom of the beam, are shown in Figures 5.14a and 5.14b, respectively. Though the prestressing force was calculated such that no tensile strains would be induced in the model under any loading case, some tensile strains were induced in the top of the curb near the end diaphragm (see Figure 5.14a). These tensile strains can be eliminated by applying the prestressing force in the center of the curb rather than the bottom portion of the curb where it creates local negative moment in the curb. From Figure 5.14b, one observes that even under full service load there are no

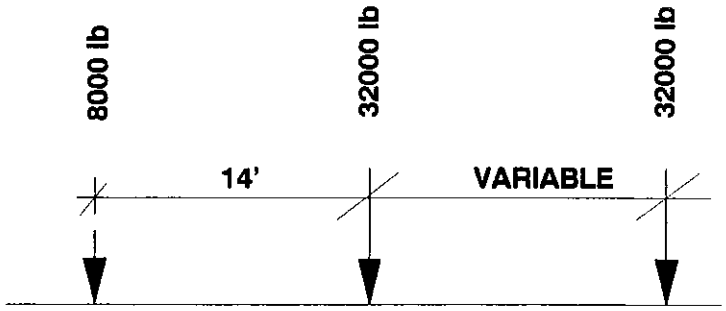

(a) Truck load as defined by AASHTO [1]

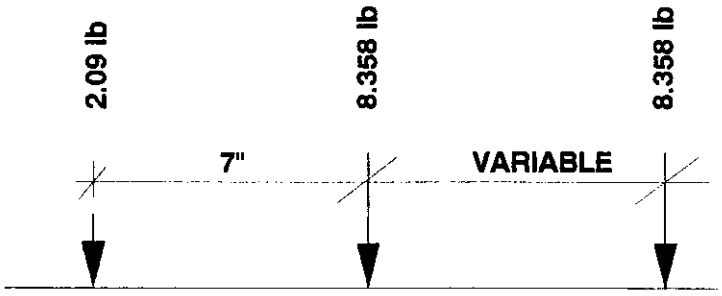

(b) Scaled truck load multiplied by Impact Factor

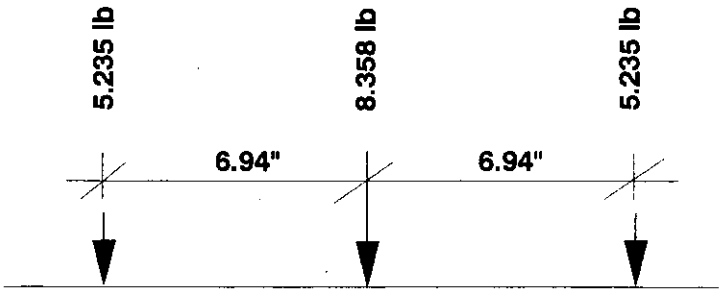

(c) Modified truck load

Figure 5.13. Various truck loadings

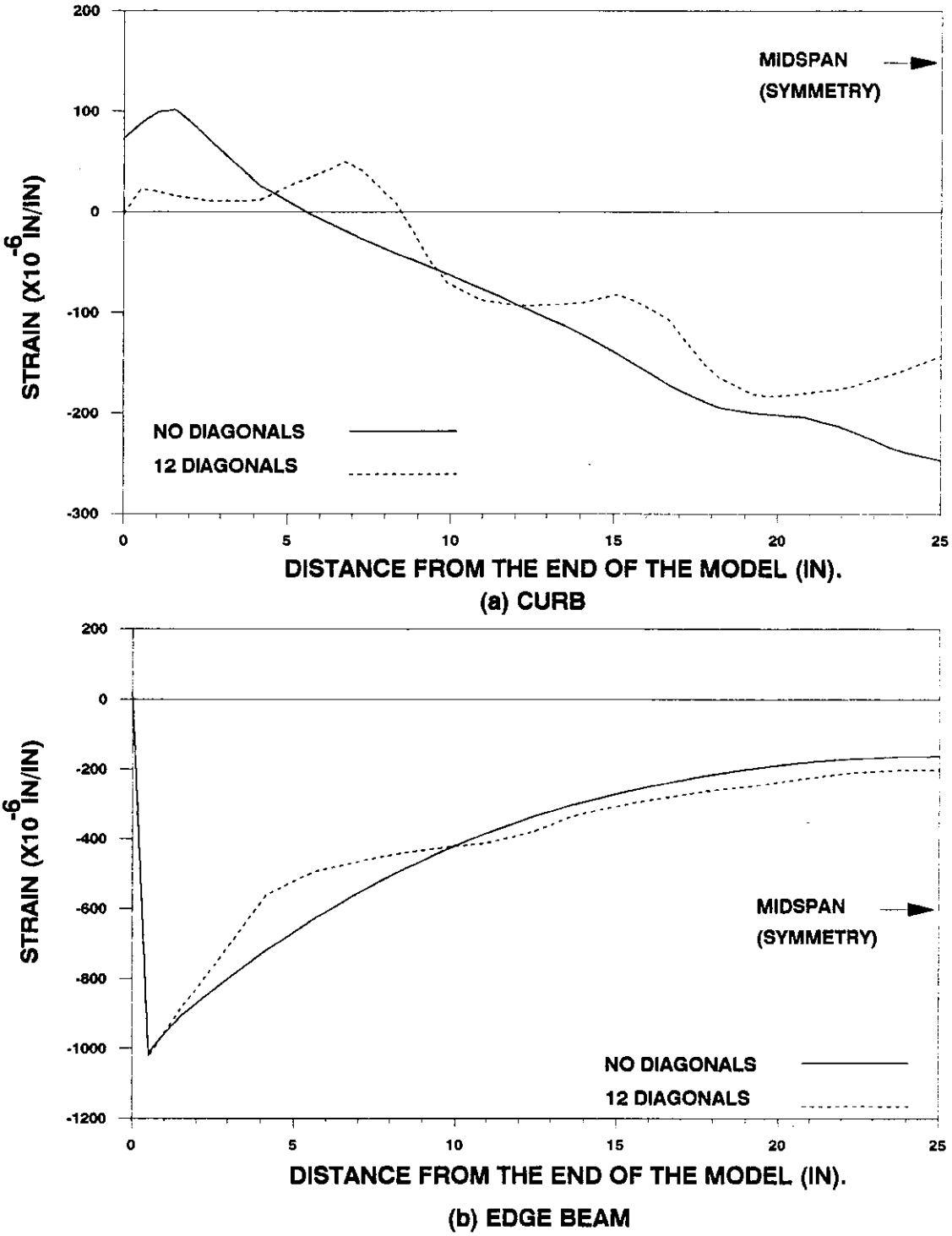

Figure 5.14. Longitudinal strain distribution along top of the curb and bottom of beam: truck at midspan, prestressing force applied

tensile strains in the bottom of the beam. This illustrates that the approximation of the integrated deck and folded plate cross section as a simple rectangular cross section is adequate for estimating the required prestressing force.

Longitudinal and transverse strains across the deck under live and dead loads and the applied prestressing force are shown in Figures 5.15a and 5.15b, respectively. The longitudinal strains across the deck, with and without the diagonals are nearly equal (see Figure 5.15a); this was observed even earlier in Figure 5.5. Hence, it can be concluded from Figures 5.5 and 5.15a that even the effect of the prestressing force in the deck does not vary with the presence or absence of diagonal members. However, as shown in Figure 5.15b the tensile transverse strains in the top of the deck are reduced by approximately 50% when diagonals are used to connect the curb and the beam. Also, by comparing the deflection of the deck at midspan as shown in Figure 5.16, the advantage of connecting the curb to the beam with diagonals is obvious. The differential deflection of the deck is minimized and the cross section is forced to act as one unit. The advantage of connecting the curbs to the beams with diagonals cannot be truly appreciated by comparing the longitudinal strains in the deck, but it is very evident when the transverse strains and deflections are compared. Figures 5.17a and 5.17b show the deflection of the beam and the curb, respectively under dead and live loads and applied prestressing force. When the curb and the beam are connected by diagonal elements, not only are their deflections reduced, but they form a truss along with the diagonals and both deflect the same amount. The same observations were made when a single concentrated load was used (see section 5.2.2).

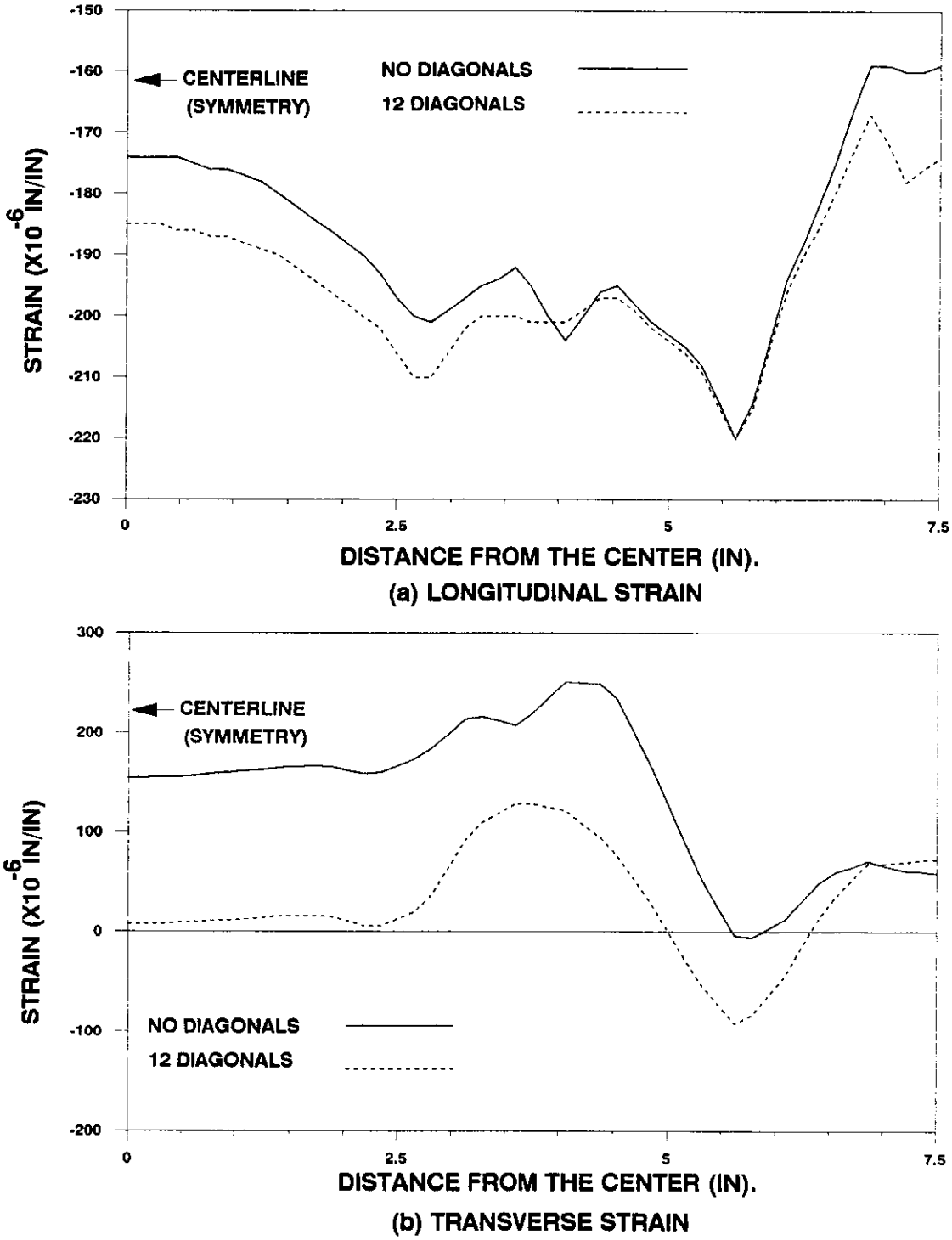

Figure 5.15. Longitudinal and transverse strain distribution on top of deck along section G: truck at midspan, prestressing force applied

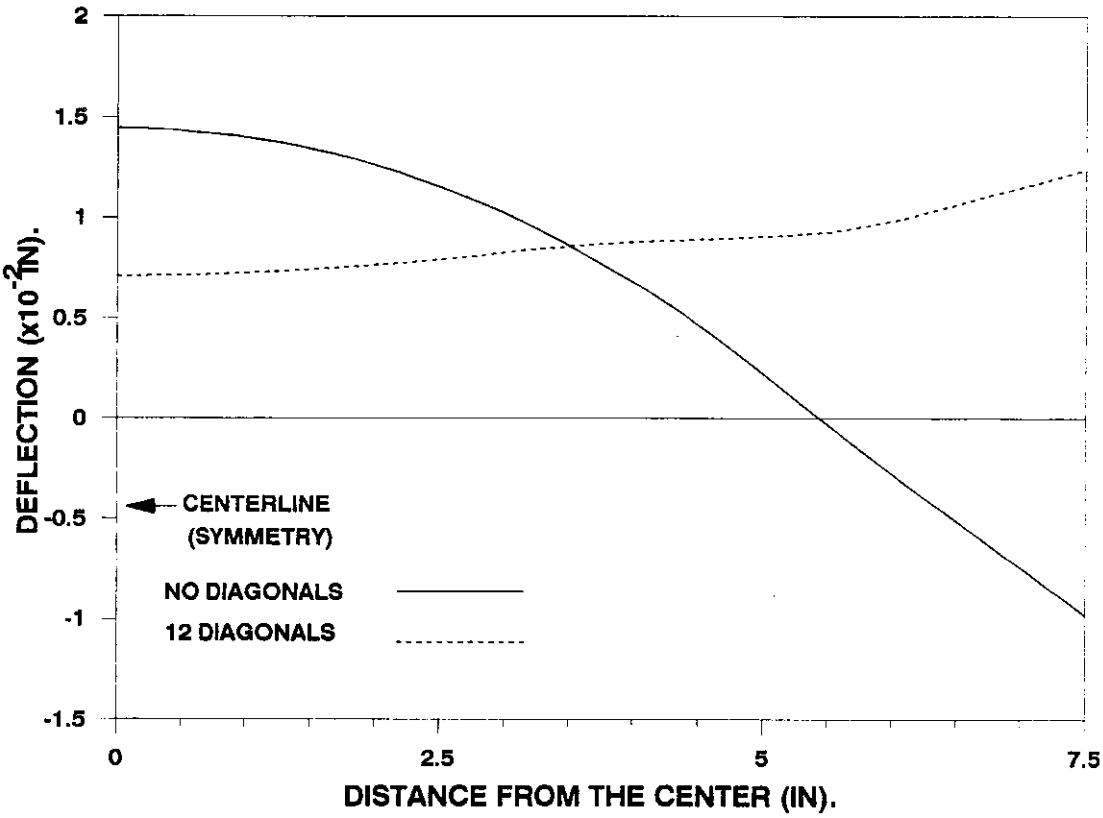

Figure 5.16. Deflection across the deck at midspan: truck at midspan, prestressing force applied

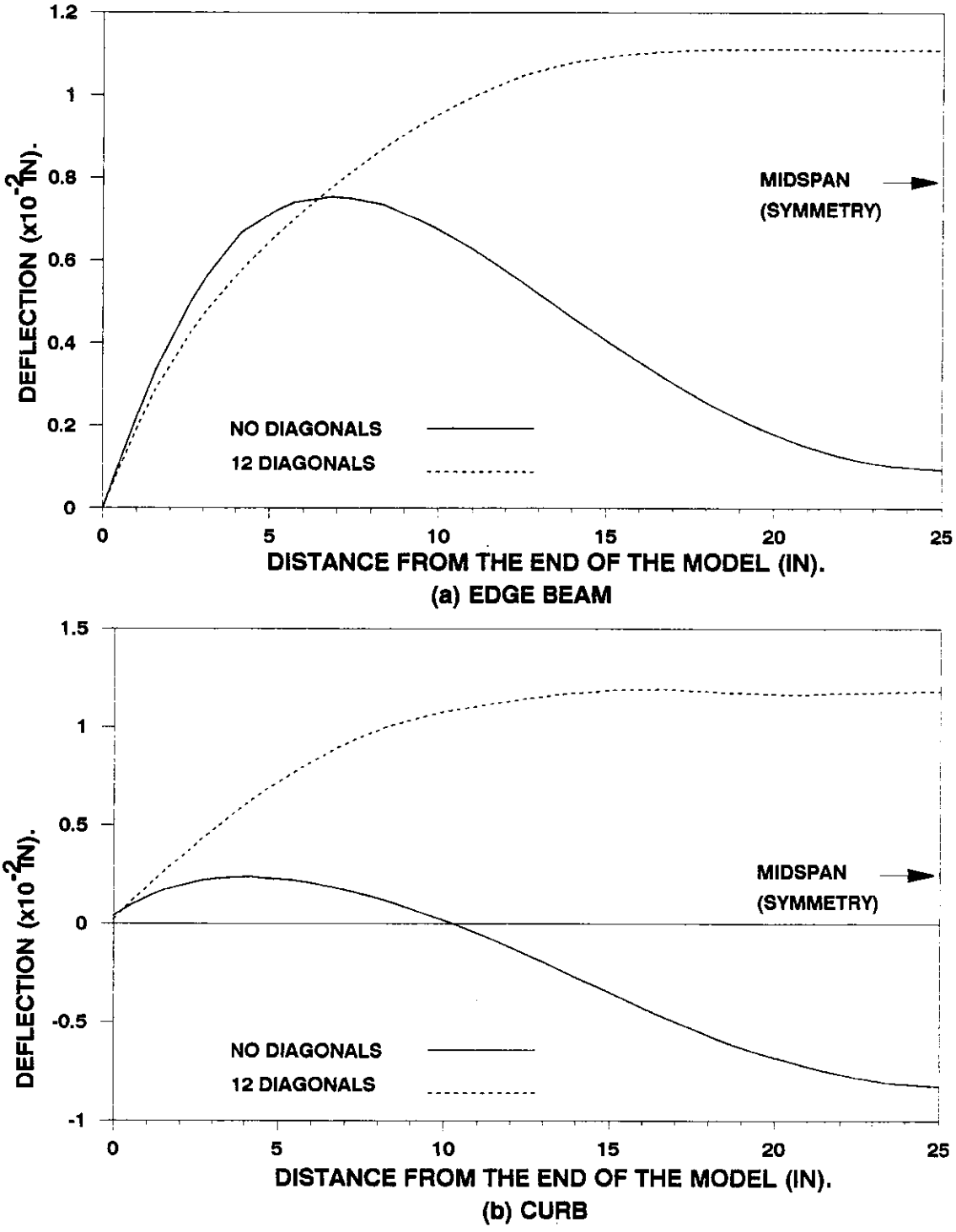

Figure 5.17. Deflection along the beam and the curb: truck at midspan, prestressing force applied

6. SUMMARY AND CONCLUSIONS

6.1. Summary

The closing of a bridge for maintenance or repairs always causes costly delays and inconvenience to the travelling public. In particular, long span bridges are more difficult to replace quickly. Needed today is an alternative bridge system which is capable of supporting current traffic volumes and is economical and fast to construct even for long spans. An integrated deck and folded plate structure which combines the advantages of prefabricated element systems and segmental construction, and has high torsional stiffness like a box girder bridge was suggested and investigated for use as abridge.

A 1:24 scale Plexiglass model of an integrated deck and folded plate bridge was constructed to simulate a 100 ft. long, 30 ft. wide, two lane simply supported single span bridge. Provisions were made to apply prestressing force to the Plexiglass model and to test the model with and without the 6 diagonal members connecting the curbs and the edge beams. The Plexiglass used in the model was experimentally calibrated to determine the value of Young's modulus of elasticity and Poisson's ratio. The response of the structure under a single concentrated load of 7.5 lb placed at several locations was documented.

A finite element analysis of the bridge model was accomplished utilizing the ANSYS finite element computer code. Three dimensional isoparametric solid elements were used to model the Plexiglass bridge and the post - tensioning tendons were modelled using the three dimensional truss elements. The finite element analysis was verified with the experimental

results after which the finite element model was modified to study the effect of using more diagonal members for connecting the curbs and the beams. The finite element technique was also employed to analyze the structure under prestressing force, dead load and AASHTO truck loads.

6.2. Conclusions

Based on the results of this investigation the following conclusions can be made:

1) The bridge deck behaves like a one way continuous slab in the transverse direction. Longitudinal strains under dead and live loads are negligible when there is no prestressing force.
2) In the absence of the diagonal members, the deck behaves more like a double cantilevered plate and there are large transverse strains in the deck and the inclined plates for loads applied near the curbs.
3) After the addition of diagonal members, the deck behaves more like a continuous slab on four elastic supports and the transverse strains in the deck and the inclined plates are reduced significantly for loads applied near the curbs.
4) The addition of the diagonal truss members reduces the overall deflection of the structure and results in higher torsional stiffness.
5) Connecting the curbs to the beams with diagonal truss members has more effect on improving the structural behavior of the section under loads applied near the curbs than under loads applied near the center of the deck.

6) Due to the high creep strain in Plexiglass, maintaining a constant prestressing force was difficult. Hence, it was difficult to reproduce experimental test results when prestressing force was applied and thus, tests results with prestressing force applied were unreliable.

7) Using beam theory is an adequate approximation for estimating the required prestressing force for the integrated deck and folded plate cross section.

6.3. Recommendations for continued study

1) Study and document the behavior of continuous span, integrated folded plate deck bridge to check feasibility of cross section for use in continuous span bridges.

2) Study the economic advantages and practical feasibility of using the integrated deck and folded plate bridge structure.

3) Develop guidelines for the design and construction of the proposed bridge structure.

REFERENCES

1. American Association of State Highway and Transportation Officials (AASHTO). "Standard Specifications for Highway Bridges," 13th Ed. AASHTO, Washington, D.C., 1983.
2. Engineering News Record, McGraw Hill Book Company, New York, NY, Jan., 1990.
3. Andrey, D., "Analytical Investigation of Shell Structures for Emergency Bypass Bridges," Thesis, Iowa State University, Ames, IA, 1987.
4. Wassef, W.G., "Analytical and Experimental Investigation of Shell Structures Utilized as Bridges," Doctoral Dissertation, Iowa State University, Ames, IA, 1991.
5. Klaiber, F. W., Gutzwiller, M. J. and Lee, R. H., "Analytical and Model Studies of Prestressed Folded Plates," Journal of the Structural Division, ASCE, Vol. 99, No. ST6, Proc. Paper 9818, Jun., 1973.
6. Brough, J. C., Jr., and Stephens, B. H., Jr., "Long Span Prestressed Concrete Folded Plate Roofs," Journal of the Structural Division, ASCE, Vol. 86, No. ST10, Proc. Paper 2630, Oct., 1960.
7. Glanville, J. I., "Full-Scale Pretensioned Folded Plates Test - Loaded to Failure," ACI Journal, Proceedings, American Concrete Institute, Vol. 60, No. 3, Mar., 1963.
8. Goble, G. G., "Analysis of Folded Plate Structures," Journal of the Structural Division, ASCE, Vol. 90, No. ST1, Proc. Paper 3797, Feb., 1964.

9. Carpenter, J. E., Roll, F. E. and Zelman, M. I., "Techniques and Materials for Structural Models - Models for Concrete Structures," American Concrete Institute Publication SP-24, Detroit, MI, 1970

10. Carpenter, J. E., Magura, D. D., and Hanson, N. W., "Structural Model Testing - Techniques for Models of Plastic," Journal of the Portland Cement Association Research and Development Laboratories, Vol. 6, No. 2, May, 1964.

11. Hood, J. A., "An Investigation of a Curved Single Cell Box Girder Bridge," Doctoral Dissertation, University Of Auckland, Auckland, New Zealand, 1976.

12. Murphy, G., "Similitude in Engineering," The Ronald Press Company, New York, 1950.

13. Micro Measurements, "Catalog 500," Measurements Group, Raleigh, NC.

14. Micro Measurements, "Technical Note - TN502," Measurements Group, Raleigh, NC.

15. De Salvo, G. J., and Swanson, J. A., "ANSYS Engineering Analysis System User's Manual," Vols. I & II, Swanson Analysis System, Inc., Houston, PA, 1985.

ACKNOWLEDGEMENTS

The author extends his sincere appreciation and commendation to his major professors, Dr. F. W. Klaiber and Dr. F. Fanous for their assistance and valuable guidance during the research work and the writing of this thesis. The author would also like to express his gratitude to professor Dr. L. W. Zachry for his guidance and for serving as a graduate committee member. The author expresses his gratitude to Dr. J. Scalzi of the National Science Foundation for providing the funds for this work and for his continuous support.

The author is forever indebted to his parents for their continued love and support throughout his education.